International Journal of Physical Sciences

Volume 9 Number 3 9 February, 2014
ISSN 1992-1950

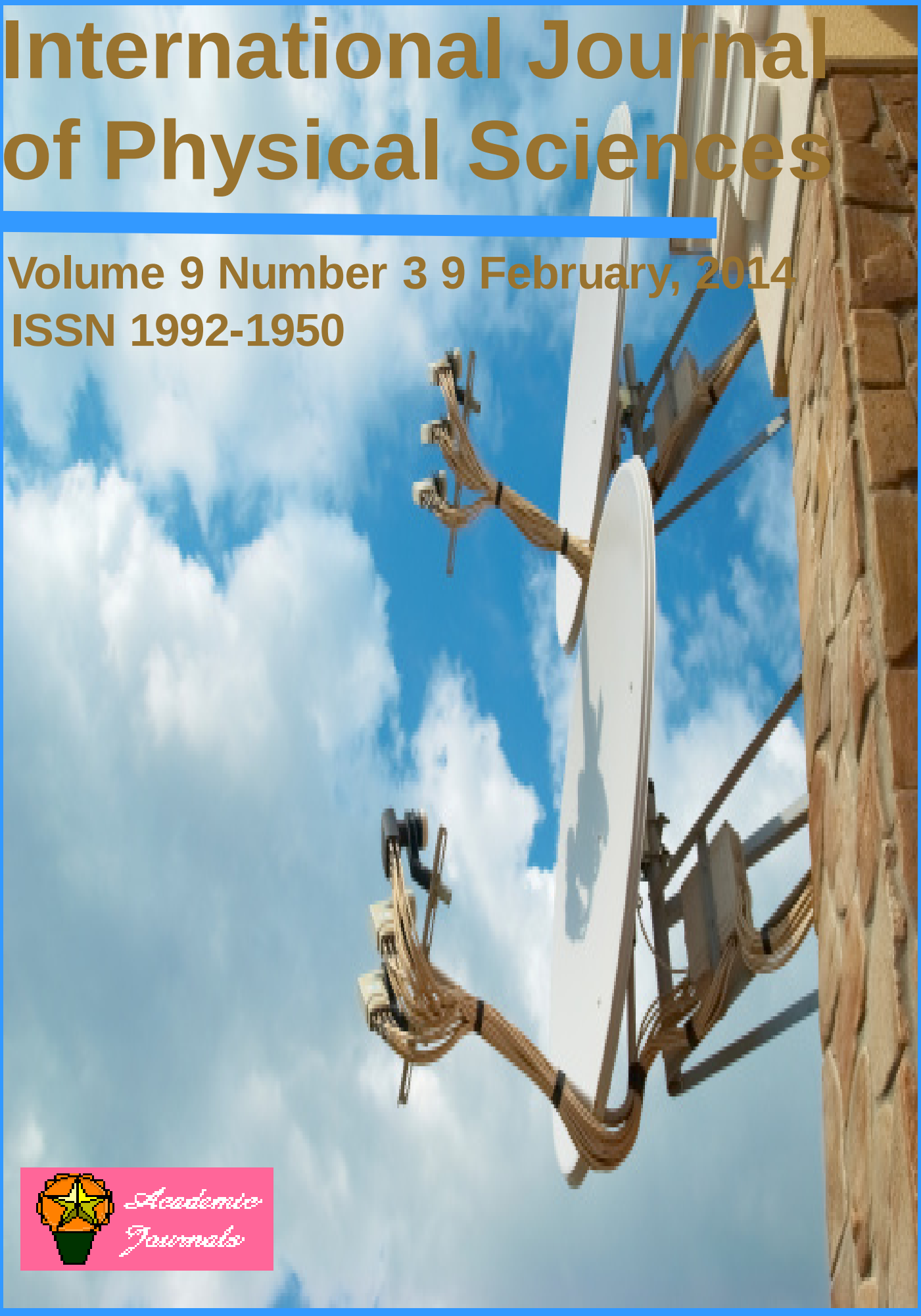

Academic Journals

ABOUT IJPS

The **International Journal of Physical Sciences (IJPS)** is published weekly (one volume per year) by Academic Journals.

International Journal of Physical Sciences (IJPS) is an open access journal that publishes high-quality solicited and unsolicited articles, in English, in all Physics and chemistry including artificial intelligence, neural processing, nuclear and particle physics, geophysics, physics in medicine and biology, plasma physics, semiconductor science and technology, wireless and optical communications, materials science, energy and fuels, environmental science and technology, combinatorial chemistry, natural products, molecular therapeutics, geochemistry, cement and concrete research, metallurgy, crystallography and computer-aided materials design. All articles published in IJPS are peer-reviewed.

Submission of Manuscript

Submit manuscripts as e-mail attachment to the Editorial Office at: ijps@academicjournals.org. A manuscript number will be mailed to the corresponding author shortly after submission.

For all other correspondence that cannot be sent by e-mail, please contact the editorial office (at ijps@academicjournals.org).

The International Journal of Physical Sciences will only accept manuscripts submitted as e-mail attachments.

Please read the **Instructions for Authors** before submitting your manuscript. The manuscript files should be given the last name of the first author.

Editorial Board

Instructions for Author

Electronic submission of manuscripts is strongly encouraged, provided that the text, tables, and figures are included in a single Microsoft Word file (preferably in Arial font).

The **cover letter** should include the corresponding author's full address and telephone/fax numbers and should be in an e-mail message sent to the Editor, with the file, whose name should begin with the first author's surname, as an attachment.

Article Types

Three types of manuscripts may be submitted:

Regular articles: These should describe new and carefully confirmed findings, and experimental procedures should be given in sufficient detail for others to verify the work. The length of a full paper should be the minimum required to describe and interpret the work clearly.

Short Communications: A Short Communication is suitable for recording the results of complete small investigations or giving details of new models or hypotheses, innovative methods, techniques or apparatus. The style of main sections need not conform to that of full-length papers. Short communications are 2 to 4 printed pages (about 6 to 12 manuscript pages) in length.

Reviews: Submissions of reviews and perspectives covering topics of current interest are welcome and encouraged. Reviews should be concise and no longer than 4-6 printed pages (about 12 to 18 manuscript pages). Reviews are also peer-reviewed.

Review Process

All manuscripts are reviewed by an editor and members of the Editorial Board or qualified outside reviewers. Authors cannot nominate reviewers. Only reviewers randomly selected from our database with specialization in the subject area will be contacted to evaluate the manuscripts. The process will be blind review.

Decisions will be made as rapidly as possible, and the journal strives to return reviewers' comments to authors as fast as possible. The editorial board will re-review manuscripts that are accepted pending revision. It is the goal of the IJPS to publish manuscripts within weeks after submission.

Regular articles

All portions of the manuscript must be typed double-spaced and all pages numbered starting from the title page.

The Title should be a brief phrase describing the contents of the paper. The Title Page should include the authors' full names and affiliations, the name of the corresponding author along with phone, fax and E-mail information. Present addresses of authors should appear as a footnote.

The Abstract should be informative and completely self-explanatory, briefly present the topic, state the scope of the experiments, indicate significant data, and point out major findings and conclusions. The Abstract should be 100 to 200 words in length.. Complete sentences, active verbs, and the third person should be used, and the abstract should be written in the past tense. Standard nomenclature should be used and abbreviations should be avoided. No literature should be cited.

Following the abstract, about 3 to 10 key words that will provide indexing references should be listed.

A list of non-standard **Abbreviations** should be added. In general, non-standard abbreviations should be used only when the full term is very long and used often. Each abbreviation should be spelled out and introduced in parentheses the first time it is used in the text. Only recommended SI units should be used. Authors should use the solidus presentation (mg/ml). Standard abbreviations (such as ATP and DNA) need not be defined.

The Introduction should provide a clear statement of the problem, the relevant literature on the subject, and the proposed approach or solution. It should be understandable to colleagues from a broad range of scientific disciplines.

Materials and methods should be complete enough to allow experiments to be reproduced. However, only truly new procedures should be described in detail; previously published procedures should be cited, and important modifications of published procedures should be mentioned briefly. Capitalize trade names and include the manufacturer's name and address. Subheadings should be used. Methods in general use need not be described in detail.

Results should be presented with clarity and precision. The results should be written in the past tense when describing findings in the authors' experiments. Previously published findings should be written in the present tense. Results should be explained, but largely without referring to the literature. Discussion, speculation and detailed interpretation of data should not be included in the Results but should be put into the Discussion section.

The Discussion should interpret the findings in view of the results obtained in this and in past studies on this topic. State the conclusions in a few sentences at the end of the paper. The Results and Discussion sections can include subheadings, and when appropriate, both sections can be combined.

The Acknowledgments of people, grants, funds, etc should be brief.

Tables should be kept to a minimum and be designed to be as simple as possible. Tables are to be typed double-spaced throughout, including headings and footnotes. Each table should be on a separate page, numbered consecutively in Arabic numerals and supplied with a heading and a legend. Tables should be self-explanatory without reference to the text. The details of the methods used in the experiments should preferably be described in the legend instead of in the text. The same data should not be presented in both table and graph form or repeated in the text.

Figure legends should be typed in numerical order on a separate sheet. Graphics should be prepared using applications capable of generating high resolution GIF, TIFF, JPEG or Powerpoint before pasting in the Microsoft Word manuscript file. Tables should be prepared in Microsoft Word. Use Arabic numerals to designate figures and upper case letters for their parts (Figure 1). Begin each legend with a title and include sufficient description so that the figure is understandable without reading the text of the manuscript. Information given in legends should not be repeated in the text.

References: In the text, a reference identified by means of an author‘s name should be followed by the date of the reference in parentheses. When there are more than two authors, only the first author‘s name should be mentioned, followed by ’et al‘. In the event that an author cited has had two or more works published during the same year, the reference, both in the text and in the reference list, should be identified by a lower case letter like ’a‘ and ’b‘ after the date to distinguish the works.

Examples:

Abayomi (2000), Agindotan et al. (2003), (Kelebeni, 1983), (Usman and Smith, 1992), (Chege, 1998; 1987a,b; Tijani, 1993,1995), (Kumasi et al., 2001)

References should be listed at the end of the paper in alphabetical order. Articles in preparation or articles submitted for publication, unpublished observations, personal communications, etc. should not be included in the reference list but should only be mentioned in the article text (e.g., A. Kingori, University of Nairobi, Kenya, personal communication). Journal names are abbreviated according to Chemical Abstracts. Authors are fully responsible for the accuracy of the references.

Examples:

Ogunseitan OA (1998). Protein method for investigating mercuric reductase gene expression in aquatic environments. Appl. Environ. Microbiol. 64:695-702.

Gueye M, Ndoye I, Dianda M, Danso SKA, Dreyfus B (1997). Active N2 fixation in several Faidherbia albida provenances. Ar. Soil Res. Rehabil. 11:63-70.

Charnley AK (1992). Mechanisms of fungal pathogenesis in insects with particular reference to locusts. In: Lomer CJ, Prior C (eds) Biological Controls of Locusts and Grasshoppers: Proceedings of an international workshop held at Cotonou, Benin. Oxford: CAB International, pp 181-190.

Mundree SG, Farrant JM (2000). Some physiological and molecular insights into the mechanisms of desiccation tolerance in the resurrection plant Xerophyta viscasa Baker. In Cherry et al. (eds) Plant tolerance to abiotic stresses in Agriculture: Role of Genetic Engineering, Kluwer Academic Publishers, Netherlands, pp 201-222.

Short Communications

Short Communications are limited to a maximum of two figures and one table. They should present a complete study that is more limited in scope than is found in full-length papers. The items of manuscript preparation listed above apply to Short Communications with the following differences: (1) Abstracts are limited to 100 words; (2) instead of a separate Materials and Methods section, experimental procedures may be incorporated into Figure Legends and Table footnotes; (3) Results and Discussion should be combined into a single section.

Proofs and Reprints: Electronic proofs will be sent (e-mail attachment) to the corresponding author as a PDF file. Page proofs are considered to be the final version of the manuscript. With the exception of typographical or minor clerical errors, no changes will be made in the manuscript at the proof stage.

International Journal of Physical Sciences

Table of Contents: Volume 9 Number 3, 9 February, 2014

ARTICLES

academicJournals

Vol. 9(3), pp. 26-33, 9 February, 2014
DOI: 10.5897/IJPS2013.4088
ISSN 1992 - 1950 © 2014 Academic Journals
http://www.academicjournals.org/IJPS

International Journal of Physical Sciences

Full Length Research Paper

A planar microstrip metamaterial resonator using split ring dual at Ku-Band

Nitin Kumar[1]* and S. C. Gupta[2]

[1]ECE Department, Uttarakhand Technical University, Dehradun, Uttarakhand, India.
[2]ECE Department, DIT University, Dehradun, Uttarkhand, India.

Accepted 29 January, 2014

This paper introduces a new planar microstrip metamaterial resonator, the novelty of this paper lays in its unit cell design. The unit cell is formed by connecting metallic traces of two edge coupled split ring resonators to form the infinity symbol on one side of the substrate, and an array of conducting wires on the other. An RLC equivalent model of the structure is also proposed, it can be advantageous to use this model to identify the resonant frequency along with the root of the negative permeability and negative permittivity. The model shows resonance at 17 GHz. The structure was designed and simulated using EM solver Ansys HFSS, the extracted s-parameter matrix was analyzed to determine the effective permittivity, permeability and index of refraction. The structure shows negative values for effective ε, μ at resonant frequency 16.5 GHz. At frequencies where both the recovered real parts of ε and μ are simultaneously negative, the real part of the index of refraction is also found to be negative.

Key words: Microstrip metamaterial, negative refraction, permittivity, permeability, RLC circuit.

INTRODUCTION

Metamaterials, first named and theoretically discussed by Veselago (1968), are studied widely throughout the world. These are an artificially engineered material showing electromagnetic properties not readily found in naturally occurring material, such as, property of negative refractive index and artificial magnetism (Sabah, 2010; Mahmood, 2004; Sulaiman et al., 2010; Smith et al., 2001; Sharma et al., 2011). Recently work is done in direction of making a perfect lens using metamaterials (He-Xiu Xu et al., 2013a, b).

Metamaterials are often characterized in terms of their effective material properties, such as effective electric permittivity and effective magnetic permeability. Any one of these parameters, or even both of them may be simultaneously negative. The former is known as single negative material (SNG), if only effective permittivity is negative it is called Epsilon negative material (ENG), whereas if only effective permeability is negative it is called as Mu-negative material (MNG). The latter is referred to as left-handed metamaterials (LHM), double negative (DNG), or negative refractive index material (NRIM).

Artificial plasmas show negative effective permittivity for all frequencies smaller than plasma frequency of the Plasmon medium (Pendry et al., 1996). Effective negative permeability can be obtained in the well known Split-ring-resonator structure, but only for a narrow magnetic resonant frequency band (Pendry et al., 1999). In past few years, metamaterials has been a naive topic of interest among the research fraternity. Over these years various innovative structures have been reported.

This paper presents design and simulation of a new planar microstrip metamaterial resonator, exhibiting negative index of refraction. In comparison to the papers

*Corresponding author. E-mail: nitin.vnit@gmail.com

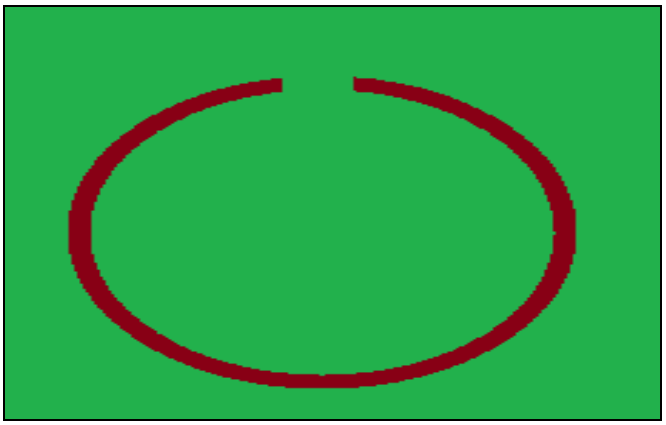

Figure 1. A Circular Split-Ring Resonator Structure (SRR).

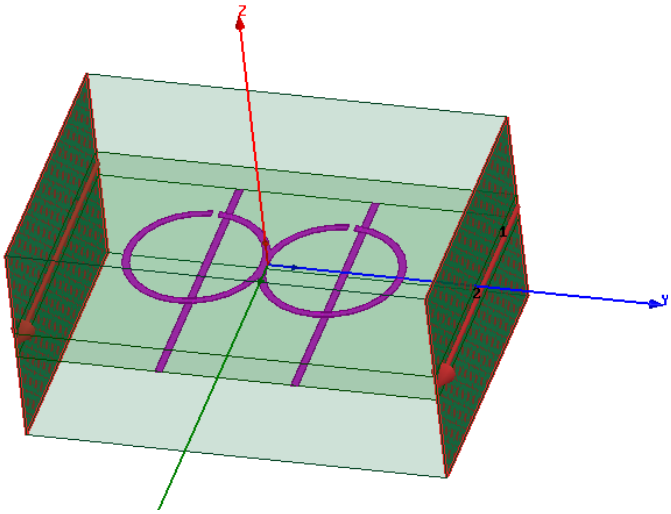

Figure 2a. Structure of Infinity Shaped Metamaterial (ISM) kept in a waveguide with wave-ports.

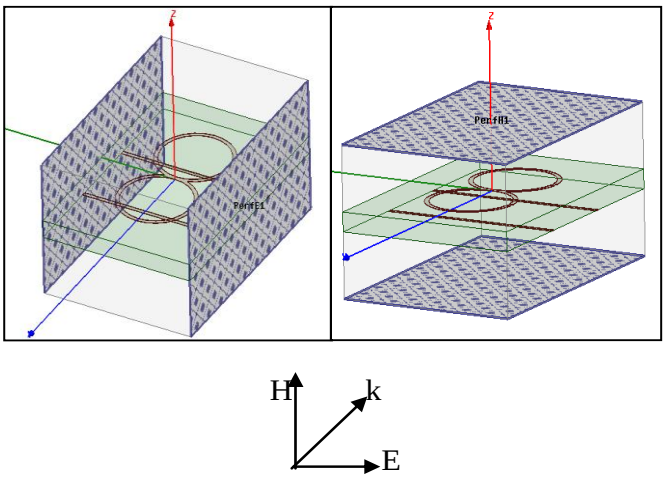

Figure 2b. Schematic diagram of ISM, showing the boundary conditions: PEC and PMC boundaries respectively.

cited here, the novelty of this paper lies in the unit cell design, where two edge coupled circular split-ring resonators are connected to form the infinity symbol and an array of straight wire conductors is also used. The overall size of the metamaterial unit is very small 6 mm × 8 mm. Since the geometry of the structure resembles the shape of mathematical symbol 'infinity' it will be referred to as Infinity Shaped Metamaterial (ISM) in rest of the paper. The structure was simulated using Ansys HFSS and the extracted s-parameter values (S_{11} and S_{21}) was analyzed to calculate index of refraction. The results promises a bandwidth of around 8 GHz (~8.5 to 16.5 GHz).

Many researchers have done the analysis of SRR unit cells and SRR arrays, and shown that SRRs behave as LC resonators that can be excited by external magnetic flux. The analysis of SRRs by accurate circuit models can be effectively used to estimate the behavior of SRR structures in a simple, efficient manner. Also, explicit relationships between electrical parameters, dimensions of the SRR structure and its frequency dependent transmission/reflection behavior may be found.

Another method called NRW technique (Suganthi et al., 2012) was also used to calculate effective permittivity and effective permeability from s-parameters, using which refractive index can be calculated. The results obtained from all techniques were compared and found in satisfactory agreement with each other.

DESIGN SETUP

Figure 1 above shows a single Circular Split-Ring Resonator, and Figure 2a shows the unit cell of Infinity Shaped Metamaterial (ISM).

It has been shown in various papers that a single SRR provides magnetic resonance and supports negative effective permeability (Pendry et al., 1999), in this paper it can be seen from Figure 2a that, ISM can be formed by connecting traces of two SRRs in edge coupled configuration in the shape of mathematical symbol 'infinity'. This structure behaves as 2 SRR's connected in series. Figure 2a also shows the ground plane, which is composed of an array of straight wire conductors instead of a continuous sheet of copper. These straight wire conductors are placed directly beneath the slit of the SRRs lying on other side of the substrate; they will provide a virtual path for the currents to continue flowing in the split rings.

As suggested by Pendry et al. (1996), the electric field should be parallel to the wire while the magnetic field should be perpendicular to the SRR. To retrieve the scattering parameters the radiation setup of the structure is done in an air filled waveguide. The electric (PEC) and magnetic (PMC) fields are defined over the walls of the waveguide in such a manner that the aforementioned conditions are satisfied, and is shown in Figure 2b. The structure is fed RF signals ranging from 15 to 18 GHz,

Table 1. Parameter table.

Parameters	Values
Substrate (Duroid (tm)) with Thickness	0.786 mm
Relative dielectric constant	1.1
Radius of outer circle of the ring	2 mm
Radius of inner circle of the ring	1.8 mm
Width of split/Width of wire conductor	0.2 mm

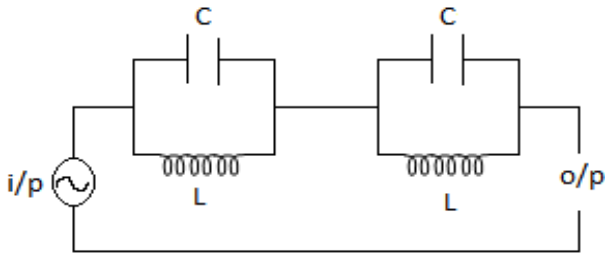

Figure 3. Simplified equivalent circuit of ISM unit cell.

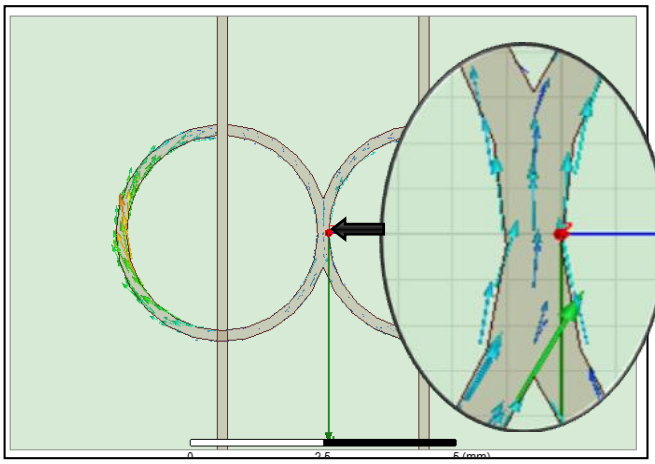

Figure 4. Distribution of current over the metallic rings, also showing the addition of current in the area common to both rings.

with the help of wave-ports (Figure 2a). The physical parameters of the structure are mentioned in Table 1.

Thus, the proposed structure ISM is a composite of split-rings and array of wires; both components are required to obtain negative effective permittivity and negative effective permeability in a single structure.

Two port equivalent circuit model of ISM

The simplified two-port equivalent circuit representation suggested for ISM unit cell is shown in Figure 3, where *L* is the self-inductance of the metal loop, which can be computed by the expressions given in (Mondher et al., 2011). The model parameter *C* is the capacitance computed for split ring calculated as:

$$C = Cpp + Cs$$

where *Cpp* and *Cs* are parallel plate and surface capacitances, respectively. The resonant frequency of the structure can be calculated by $f = {}^{1}/_{2\pi LC}$. For simplicity of design and calculations, the effect of coupling between strip used as ground and metallic SRRs is neglected; similarly the mutual coupling effect between the two SRRs connected to form 'infinity' is also neglected. Since the two metallic traces are connected together in series w.r.t the feeding, the current flowing in two rings must combine additively in the area common to both the rings. The same is verified by plotting the distribution of current over the metallic rings using HFSS, and is shown in Figure 4.

The electrical parameters of the model are computed as:

$$L = \mu_0 r\left[log\left(\frac{2r}{g}\right) + 0.9 + 0.2\left(\frac{g}{2r}\right)^2\right] \quad (1)$$

where, L represents the inductance of SRR, g represents the width of the split, and r is the average or mean radius. To calculate the total capacitance, a simple analytical approximate expression may be used. First, the surface capacitance is determined analytically by using analytical expressions for the electric field of a split-ring, and is given by (Mondher et al., 2011):

$$C_s = \frac{2\varepsilon_0(t+W)}{\pi} log\frac{4r_i}{g} \quad (2)$$

where, C_s is the surface capacitance, ε_0 permittivity of free space, w represents the width of the metallic split ring, t thickness of the metal used for split ring, r_i inner radius of the split ring, and g width of the split.

Secondly, the gap capacitance or parallel plate capacitance of the split is computed as:

$$C_{pp} = \frac{\varepsilon_0\varepsilon_r A}{g} \quad (3)$$

where, C_{pp} is the parallel plate capacitance (of the split), ε_r relative permittivity, *A* is area of the plate of capacitor

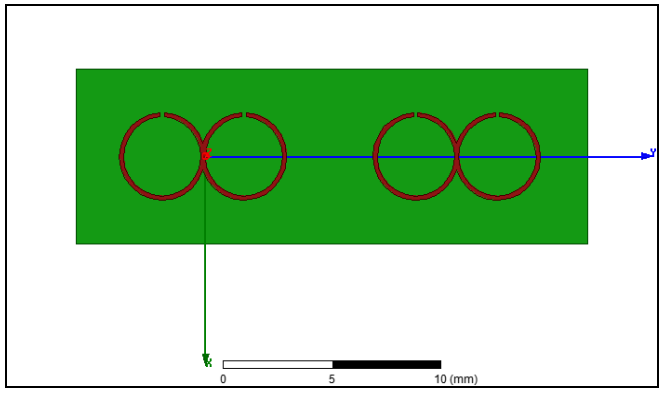

Figure 5. Array of two ISM elements.

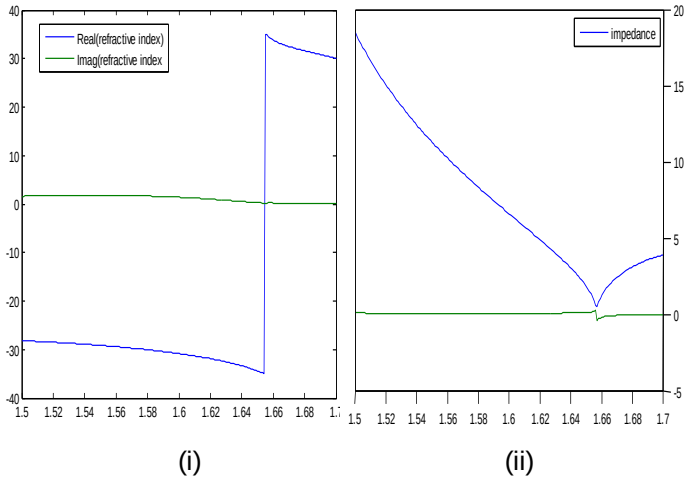

Figure 6. (i) Refractive Index (ii) Wave impedance versus Frequency.

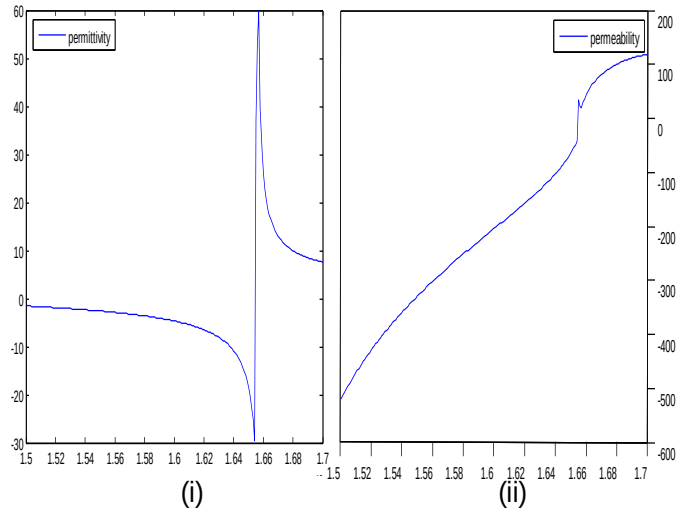

Figure 7. (i) Effective permittivity, (ii) Effective permeability versus Frequency in GHz.

(here $A=t * w$).Using the above formulae, the value of inductance and capacitance was calculated, and the resonant frequency using these values comes out to be ~17 GHz.

A linear array of two elements (shown in Figure 5) was then developed and analyzed, the coupling effects between two ISM unit cells can be described by a parallel RC circuit in the shunt branch. This coupling equivalent circuit is connected in series between two ISM blocks. The coupling parameters C_m and L_m can be computed by similar approaches used for the computation of the parameters *C* and *L* mentioned previously. The effect of mutual coupling between two ISM elements was found to be too small, and had a very little effect on the resonant frequency. Hence, it was not considered here.

SIMULATION AND RESULTS

The ISM structure was designed and simulated using EM solver Ansys HFSS. With extracted s-parameter matrix, value of refractive index *n* and wave impedance *z* was calculated using the following equations (Sabah, 2010; Smith et al., 2001).

$$n = \frac{1}{kd}\cos^{-1}\left\{\frac{1-S_{11}^2+S_{21}^2}{2S_{21}}\right\} \quad (4)$$

$$z = \pm\sqrt{\frac{(1+S_{11})^2-S_{21}^2}{(1-S_{11})^2-S_{21}^2}} \quad (5)$$

The value of effective permittivity ε and effective permeability μ then may be computed as $\varepsilon_{eff} = n/z$ and $\mu_{eff} = n * z$.

The condition Im{n}≥0 fix the choice for sign of '*n*'. Similarly the condition Re{z}≥0 fixes the choice for sign of '*z*'. An improved parameter retrieval method given in (Liu and Wang, 2012) is as follows:

$$n = \frac{ln\left(\frac{S_{21}}{1-S_{11}\frac{z-1}{z+1}}\right)}{ikd} \quad (6)$$

where, *k* is wave number, *d* is thickness of ISM unit cell.

We calculate *z* first, and then *n* can be calculated from Equation (6). All of the above formulae were programmed in MATLAB 2009a to obtain the required plots. Refractive index versus frequency curve using Equation (6) and wave impedance using Equation (5) are shown in Figures 6 and 7:

After calculating *n* and *z*, the value of effective permittivity and permeability was computed and the graphs versus frequency are shown below:

The graphs above suggests metamaterial behavior of ISM at ~16.5 GHz. Although the results above are calculated using well known techniques, one more

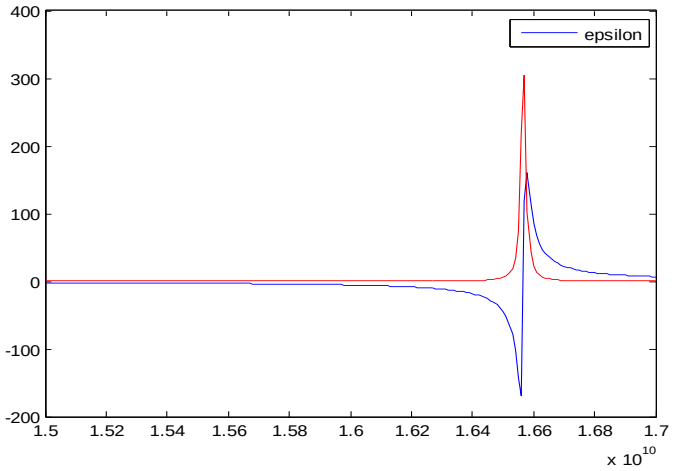

Figure 8. Effective permittivity versus Frequency in GHz.

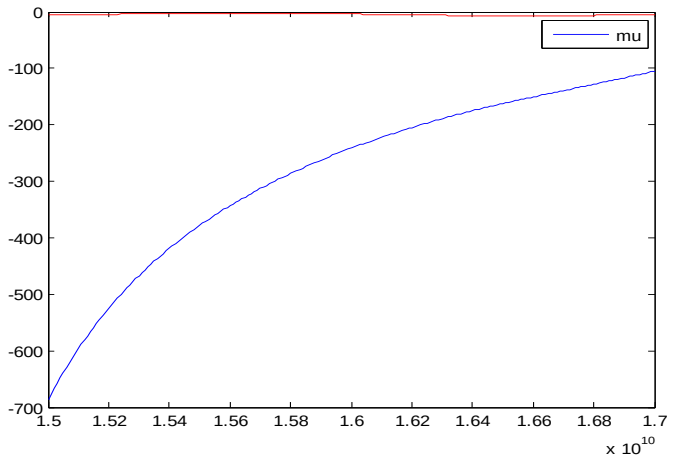

Figure 9. Effective permeability versus Frequency in GHz.

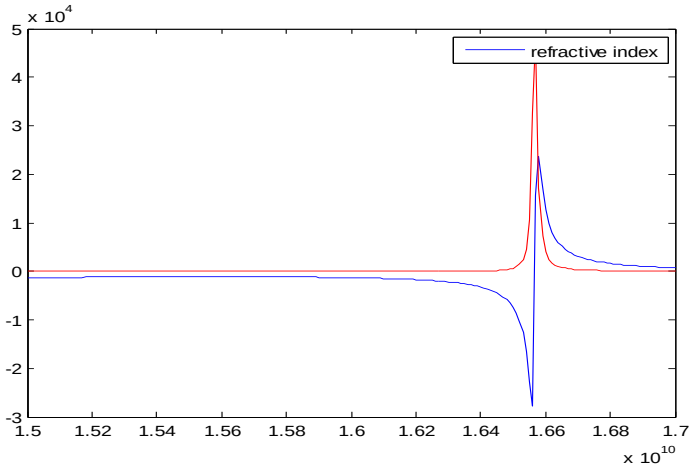

Figure 10. Refractive Index versus Frequency in GHz.

technique, the NRW parameter retrieval approach is also used in this paper to reinforce the results already obtained. A separate MATLAB code was developed based on NRW approach to find the medium properties using extracted S11 and S21 parameters. The results obtained using NRW approach shown in Figure 8 to 10 are in satisfactory agreement with those produced from Equation (4) to (6) (shown in Figures 6 and 7). The ε_{eff} and μ_{eff} of the medium are related to *S*-parameters by the Equations (7) and (8) below (Suganthi et al., 2012):

$$\varepsilon_{eff} = \frac{2}{jk_0 d}\frac{1-V_1}{1+V_1} \quad (7)$$

$$\mu_{eff} = \frac{2}{jk_0 d}\frac{1-V_2}{1+V_2} \quad (8)$$

where k_0 is a wave number equivalent to $2\pi/\lambda_0$, d is the thickness of the substrate and $V1$ and $V2$.

$$V_1 = S_{21} + S_{11} \quad (9)$$

$$V_2 = S_{21} - S_{11} \quad (10)$$

After calculating ε_{eff} and μ_{eff} using above equations, refractive index *'n'* can be computed using:

$$n = \pm\sqrt{\varepsilon_{eff} * \mu_{eff}} \quad (11)$$

Using MATLAB, graphs for effective permittivity, effective permeability, refractive index versus frequency are plotted and are shown in Figures 8 to 10:

Figure 10 shows negative value of refractive index below ~16.5 GHz. The results obtained from HFSS for ISM unit cell and for linear array of 1×2 ISM elements are shown in Figures 11 and 12.

In Figures 11 and 12 the dip in value of S_{11}(dB), shows the resonant frequency of ISM unit cell and array of 1×2 ISM elements, respectively. The resonant frequency in both cases is 16.58 and 16.5 GHz, approximately same. The graph (Figure 13(i)) shows the phase of S_{11} and S_{21}(Radians) for ISM unit cell and its array. The phase of S_{11} and S_{21} crosses each other and shows zero crossing at resonant frequency, which suggests the presence of metamaterial property. Also, the metamaterial property was preserved in case of linear array of two or more elements.

For further analysis a linear array of 10 elements was prepared to observe any deviation in resonant frequency, Figure 14 shows the structure and results for a linear array of 10 elements. From the results (Figure 13 (ii)) it may be observed that the shift in resonant frequency is too small to be considered.

The results obtained for a single ISM element, array of 1×2 ISM elements, and array of 1×10 ISM elements, all

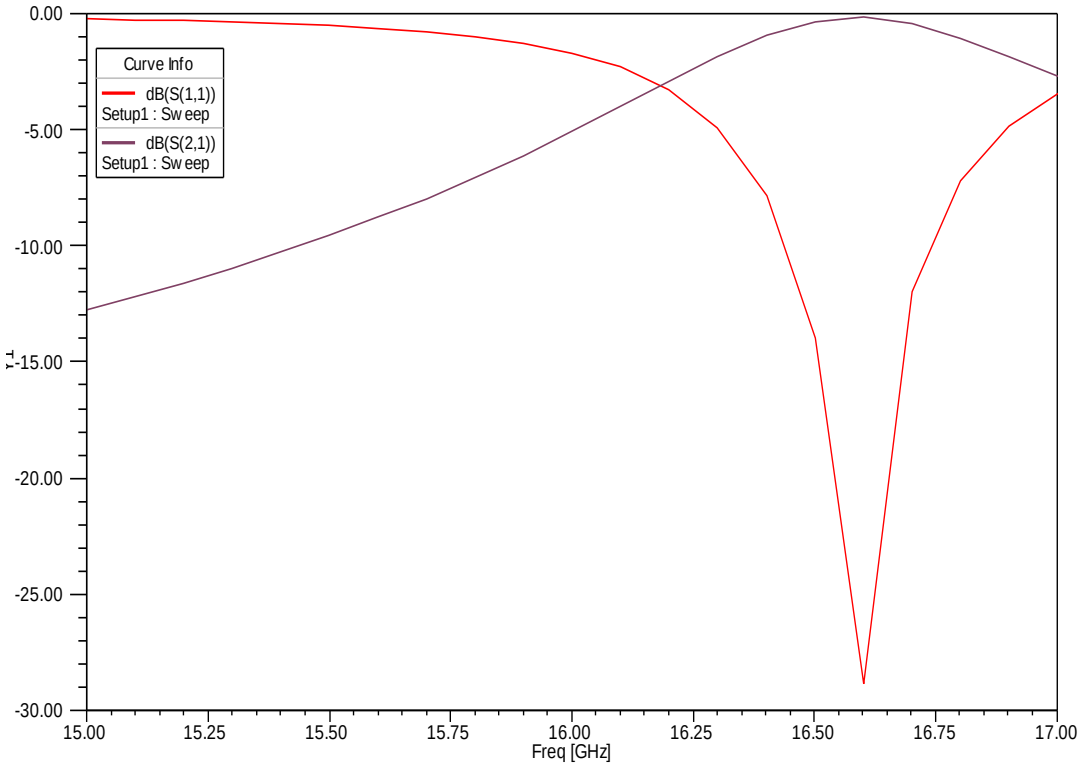

Figure 11. S_{11}(Red), S_{21}(Brown) in dB versus Frequency for ISM unit cell.

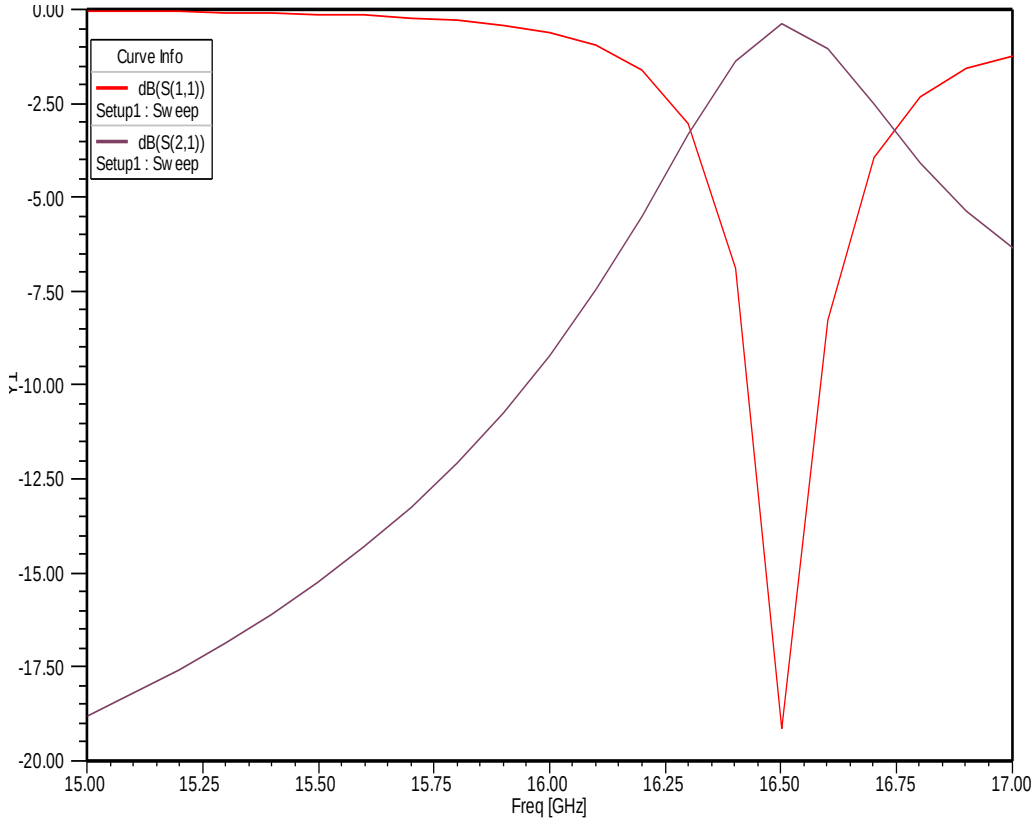

Figure 12. S_{11}(Red), S_{21}(Brown) in dB versus Frequency for 1×2 array ISM.

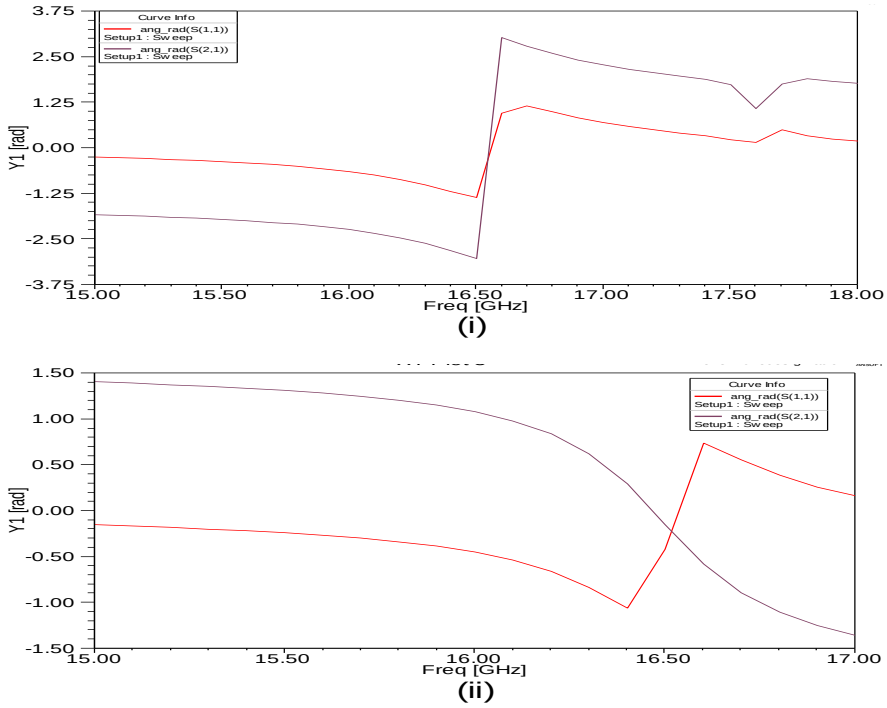

Figure 13. Phase of S11 (red), S21(brown) in radians, (i) ISM unit cell, (ii) Array of 1x2 ISM elements versus Frequency in GHz.

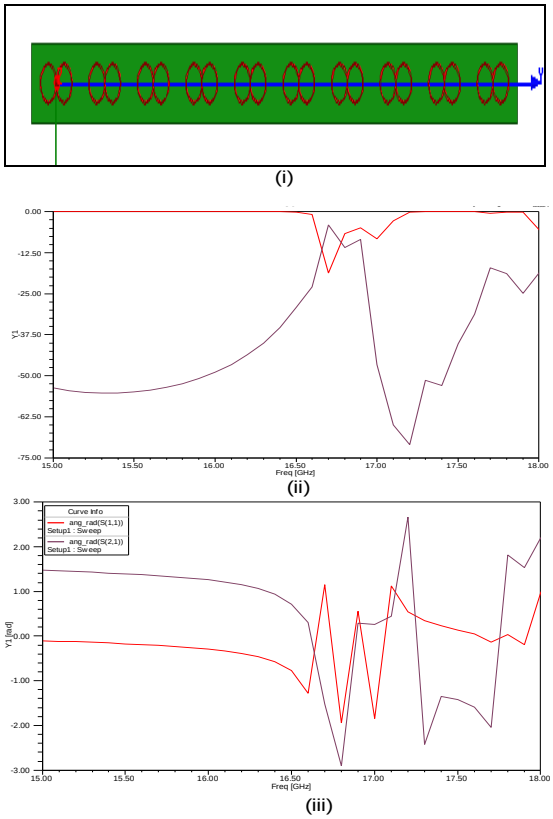

Figure 14. Linear array 10 elements (i) Structure, (ii) S11(red) and S21(brown) in dB, (iii) Phase of S11(red), S21(brown) in radians.

are in good agreement with each other and shows resonance around 16.5 GHz.

Conclusion

A new planar microstrip metamaterial resonator using circular split ring dual, connected in the shape of 'infinity' and array of straight wire conductors is presented, it exhibits the property of negative index of refraction at Ku-band. Results obtained using HFSS are verified by coding formulae for refractive index, effective permittivity, and effective permeability in MATLAB and plotting curves versus frequency. The results obtained from all the techniques mentioned in this paper are found in satisfactory agreement. In future, the presented ISM resonator can be incorporated with microstrip antennas to get highly directional beam patterns either by using it as a substrate or by using it as a metamaterial cover kept in front of the antenna; also a physical model of ISM resonator may be fabricated.

ACKNOWLEDGEMENTS

The authors are thankful to DEAL (Defense Electronics Applications Laboratory), Dehradun for extending their laboratory to use Ansoft HFSS.

REFERENCES

Mahmood SF (2004). A new miniaturized annular ring patch resonator partially loaded by a metamaterial ring with negative permeability and permittivity.IEEE Antenna Wireless Propagation Letters, 3:19-22.

Mondher L, Jamel BT, Fethi C (2011). A New Proposed Analytical Model of Circular Split Ring Resonator. Journal of Materials Science and Engineering B1, pp. 696-701.

Pendry JB, Holden AJ, Robbins DJ, Stewart WJ (1999). Magnetism from Conductors and EnhanceNonlinear Phenomena. IEEE Transactions On Microwave Theory And Techniques, 47(11):2075-2084.

PendryJB, Holden AJ, Stewart WJ, Youngs I (1996). Extremely Low Frequency Plasmons in Metallic Mesostructures.Physical Rev. Lett. 76(25);4773-4776.

Sabah C (2010). Tunable metamaterial design composed of triangular split ring resonator and wire strip for S- and C- microwave bands.Progress In Electromagnetic Research, B. 22:341-357.

Sharma V, Pattanik SS, Garg T, Devi S (2011). A microstrip metamaterial split ring resonator.Int. J. Phys. Sci. 6(4):660-663,

Smith DR, Schultz S, Markoš P, Soukoulis CM (2001). Determination of Effective Permittivity and Permeability of Metamaterials from Reflection and Transmission Coefficients.PACS Nos. 41.20.Jb, 42.25.Bs, 73.20.Mf.

Suganthi S, Raghavan S, Kumar D., Hosimin Thilagar S (2012).A Compact Hilbert Curve Fractal Antenna on Metamaterial Using CSRR.PIERS Proceedings, Kuala Lumpur, Malaysia, pp.136-140.

Sulaiman AA, Othman A, Jusoh MH, Baba NH, Awang RA, Ain MF (2010). Small Patch Antenna on Omega structure metamaterials. Europ J. Sci. Res. 43(4):527-537.

Veselago VG (1968). The Electrodynamics Of Substances With Simultaneously Negative Values Of ε And μ.Soviet Physics Uspekhi, Volume 10(4):509-514.

He-Xiu Xu, Wang, Guang-Ming Qing Qi, Mei Lv, Yuan-Yuan, Gao Xi (2013 a). Three-Dimensional Super Lens Composed of Fractal Left-Handed Materials. Advanced Optical Materials, 1(7):495–502.

He-Xiu Xu Wang, Guang-Ming Qing Qi, Mei Lv, Yuan-Yuan Gao, Xi (2013 b). Metamaterial lens made of fully printed resonant-type negative-refractive index transmission lines. Appl. Phys. Lett. 102(19):193502.

He-Xiu Xu Wang, Guang-Ming Qing Qi, Mei (2013 c). Hilbert-Shaped Magnetic Waveguided Metamaterials for Electromagnetic Coupling Reduction of Microstrip Antenna Array. IEEE Transactions On Magnetics, 49(4):1526-1529.

Liu Z , Wang P (2012). A C-Band High Gain Microstrip Antennausing Negative Permeability Metamaterial on Low Temperature Co-Fire Ceramic Substrate.Proceedings of ISAP 2012, Nagoya, Japan, pp. 878-881.

academicJournals

Vol. 9(3), pp. 34-40, 9 February, 2014
DOI: 10.5897/IJPS2013.4080
ISSN 1992 - 1950 © 2014 Academic Journals
http://www.academicjournals.org/IJPS

International Journal of Physical Sciences

Full Length Research Paper

Silver nanoparticles biogenic synthesized using an orange peel extract and their use as an anti-bacterial agent

Manal A. Awad[1], Awatif A. Hendi[2]*, Khalid M. O. Ortashi[3], Dalia F. A. Elradi[4], Nada E. Eisa[5,6], Lamia. A. Al-lahieb[7], Shorog. M. Al-Otiby[8], Nada M. Merghani[9] and Abdelelah A. G. Awad[10]

[1]King Abdullah Institute for Nanotechnology, King Saud University, Saudi Arabia.
[2]Department of Physics, Faculty of Science, King Saud University, Saudi Arabia.
[3]Department of Chemical Engineering, King Saud University, Saudi Arabia.
[4]Department of Microbiology, Faculty of Medicine, Princess Nora Bint Abdulrahman University. Saudi Arabia.
[5]Department of Physics, Al -Dammam University Kingdom of Saudi Arabia.
[6]Department of Physics, Omdurman Ahlia University, Sudan.
[7]Department of Chemistry Organic, Faculty of Science, Nature Product, Al Qassim University, Saudi Arabia.
[8]Department of Chemistry Organic, Faculty of Science, Nature Product, Princess Nora Bint Abdulrahman University, Saudi Arabia.
[9]Central Laboratory, College of Science, King Saud University, Saudi Arabia.
[10]Faculty of Animal Production, University of Khartoum, Sudan.

Accepted 29 January, 2014

Synthesis of nanoparticles by green methods with antibacterial properties is of great researchers' concern in the explored of new pharmaceutical and biomedical products. In this study, we synthesized a new product of nanosized particles of silver, non-toxic economy, clean, and conservator for energy. An environmentally friendly route is used for synthesizing silver nanoparticles (AgNPs) using an orange peel extract as both reducing and stabilizing agent at room temperature. The synthesized NPs were characterized using ultraviolet (UV)-Vis spectrophotometer, Zitasizer which measures the average size of the particles at about 91 nm, Fourier transform infrared (FT-IR) spectroscopy, scanning electron microscopy (SEM) equipped with the energy dispersive spectroscopy (EDS) and characterization using Transmission electron microscopy (TEM). The results confirmed that the orange peel extract is a very good bioreductant for the synthesis of Ag NPs and we investigated the synthesized nanoparticles as an antibacterial which showed that the biogenic synthesized AgNPs exhibit inhibition, and had significant antibacterial against both gram-positive and gram-negative bacterial strains.

Key words: Silver nanoparticles, biogenic synthesis, orange peel, anti bacterial, gram-positive, gram-negative bacteria streamers.

INTRODUCTION

Nanotechnology mainly deals with the fabrication of nanoparticles having various shapes, sizes and managing their chemical and physical parameters for further use in human benefits with their growing applications in various fields (Bhyan et al., 2007). Preparation of metal nano-sized, usually ranging in size from 1 to 100 nanometers (nm), is amongst the most emerging areas in the field of nanotechnology. Currently,

*Corresponding author. E-mail: ahindi@ksu.edu.sa.

the application of nano materials is becoming increasingly important in order to solve the problems associated with material sciences, including solar energy conversion, photonics (Calvo et al., 2006; Cao et al., 2010), catalysis (Chandan et al., 2011), microelectronics (Dastjerdi et al., 2010), antimicrobial functionalities (Du et al., 2009), and water treatment (Huang et al., 2007).

Nanoparticles usually have better or different properties than the bulk material of the same elements. The antibacterial effect of silver nanoparticles (AgNPs) is greatly enhanced because of tiny size. Nanoparticles have immense surface area relative to volume. Therefore, minuscule amounts of AgNPs can lend antimicrobial effects to hundreds of square meters of its host material. Nanomaterials are the leading requirement of the rapidly developing field of nanomedicine, and bionanotechnology. Nanoparticles are being utilized as therapeutic materials tools in infections against microbes thus, the properties of nanoparticles and their effect on microbes are essential to clinical applications. Among noble metal nanoparticles, AgNPs have received considerable attention owing to their attractive physicochemical properties (Ip et al., 2006).

The AgNPs have various and important applications. Historically, silver has been known having a disinfecting effect and has been found in applications ranging from traditional medicines to culinary items. It has been reported that AgNPs are non-toxic to human and most effective against bacteria, virus and other eukaryotic micro-organism at low concentrations and without any side effects (Jeong et al., 2005; Kamyar et al., 2012). Moreover, several salts of silver and their derivatives are commercially manufactured as antimicrobial agents (Khandelwal et al., 2010). A small concentration of silver is safe for human cells, but lethal for micro organisms (Krutyakov et al., 2008). Antimicrobial capability of AgNPs allows them to be suitably employed in numerous household applications such as textiles disinfection in water treatment, food storage containers, home appliances and in medical devices (Marambio-Jones and Hoek, 2010). The most important application of silver and AgNPs is in medical industry such as tropical ointments to prevent infection against burn and open wounds (Muhammad et al., 2012).

Biological synthesis of nanoparticles by plant extracts is at present under exploitation as some researchers worked on it (Palanivel et al., 2013; Savage and Diallo, 2005) and testing for antimicrobial activities (Savithramma et al., 2011; Saxena et al., 2010; Setua et al., 2007). For the last two decades, extensive work has been done to develop new drugs from natural products because of the resistance of micro-organisms to the existing drugs. Nature has been an important source of a products currently being used in medical practice (Sharma et al., 2009).

A number of synthetic methods have been employed for the synthesis of silver-based nanoparticles involving physical, chemical (Singh et al., 2010) and biochemical techniques (Sinha et al., 2009). Chemical reduction method is widely used to synthesize AgNPs because of its readiness to generate AgNPs under gentle conditions and its ability to synthesize AgNPs on a large scale (Thirumurgan et al., 2010). However, these chemical synthesis methods employ toxic chemicals in the synthesis route which may have adverse effect in the medical applications and hazard to environment. Therefore, preparation of AgNPs by green synthesis approach has advantages over physical and chemical approaches as it is environmental friendly, cost effective and the most significant advantage is that the conditions of high temperature, pressure, energy and no toxic chemicals are required in this synthesis protocol (Thirumurguan et al., 2009; Yugang et al., 2003).

In this present work, we report the biogenic synthesis of AgNPs by using waste biomaterial orange peel extract, which was used as green reducing agent and stabilizer. The efficacy of the synthesized AgNPs as antibacterial agent was studied.

EXPERIMENTAL

Chemicals materials and bio extract

For green synthesis of AgNPs, the reagent in this work is of analytical grade and is used as received without further purification. Silver nitrate ($AgNO_3$) from Techno Pharmchem, India is used. Orange peel was washed and cut into small pieces, then boiled with deionized water for 3min then filtered.

Synthesis of silver nanoparticles

Green AgNPs were synthesized by bio reduction of Ag^+ by using fresh suspension of (5 ml) orange peel extract (greenish in color). The emulsion color was turned to dark brown after adding to 1 mM $AgNO_3$ and stirring at room temperature.

Microorganisms and antibacterial activity method

Pure culture of *Escherichia coli, Pseudomonas aeruginosa, Klebsiella pneumoneae* and *Salmonella* are types of bacteria. The antibacterial activities of biosynthesized AgNPs were carried out by disc diffusion method. Nutrient agar medium plates were prepared, sterilized and solidified. After solidification, bacterial cultures were swabbed on these plates. The sterile discs were dipped in AgNPs solution (5 mg/ml) and placed in the nutrient agar plate and kept for incubation at 37°C for 24 h. Zones of inhibition for control, were measured. The experiments were repeated 3 times and mean values of zone diameter were determined (Jeong et al., 2005).

Characterization of biogenic silver nanoparticles

Biogenic AgNPs were characterized spectrophotometrically using ultraviolet (UV)-Vis spectroscopy analyses as function of time at room temperature using Perkin Elmer UV-Vis spectrometer, Nicolet 6700, Fourier transform infrared (FT-IR) spectrophotometer was recorded, the size of synthesized AgNPs was analyzed through

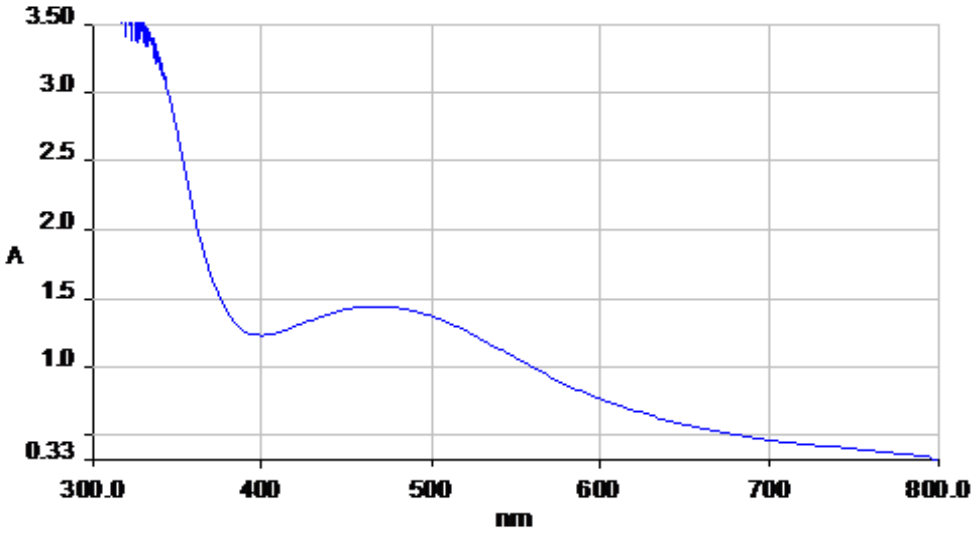

Figure 1. UV-vis spectra of reduced Ag ions to AgNPs with orange peel extract.

Zetasizer, Nano series, HT Laser, ZEN3600 from Molvern Instrument, UK, Scanning electron microscopy (SEM) has been employed to characterize the shape and morphologies of formed biogenic synthesized of AgNPs, JEOL-FE-SEM, and Energy dispersive spectrometer (EDS) analysis for the confirmation of elemental silver was carried out for the detection of elemental silver. The samples were dried at room temperature and then analyzed for samples composition of the synthesized nanoparticles. Elemental analysis on single particles was carried out using Oxford Instrument, Incax-act, equipped with SEM. Transmission electron microscopy (TEM) has been employed to characterize the size, shape and morphologies of formed biogenic synthesized of AgNPs, which was prepared by drop of AgNPs solution on carbon coated copper grid and the film on grid was dried. The TEM was operated and the measurements were performed at accelerating voltage of 100 KV.

RESULTS AND DISCUSSION

The biogenic synthesis of AgNPs by an orange peel extract was carried out. Silver nitrate used has distinctive properties such as good conductivity, catalytic and chemical stability. The formation of AgNPs was found to be successful as suggested by initial changes in color. It is well known that AgNPs exhibit brown color in aqueous solution due to excitation of surface plasmon vibrations in AgNPs.

The synthesis of green AgNPs had been confirmed by measuring the UV-Vis spectrum of colloidal solution which has absorbance peak at 466 nm; and the expanding of peak indicated that the particles are mono-dispersed as shown in Figure 1.

The FT-IR measurements were provided to describe and confirm the possible formation of bio reduction and efficient stabilization of green synthesized AgNPs by using an orange peel extract. The reduction compounds of the extract were confirmed by FT-IR spectra. FT-IR bands of orange peel were inferred at 3270.82, and 1634.24cm^{-1} in blue color (Figure 2) and FT-IR spectrum of the AgNPs shows peaks at 3260.70, 1634.62, 1376.62 and 1243.76 cm^{-1} in red color. Intense absorption is observed at 1634.24 cm^{-1} and is characteristic of the C=C stretching aromatic ring and this result agree with the result of the Thin layer chromatography (TLC) test, which refers to the active ingredient in the orange peel that causes the reduction of Ag^{+} ions, we found that the effective group is Flavonoids which led to the bio reduction of aqueous silver ions (Ag^{+}).

As shown in Figure 3, the average size of the formed biogenic AgNPs was measured by Zitasizer and it was 91.89 nm with monodispersity.

Figure 4a and b illustrate TEM images recorded at high magnification. Morphology of the AgNPs synthesized by using an orange peel extract indicates that the nanoparticles are spherical in shape with a smooth surface morphology.

SEM is shown in Figure 5a was employed to analyze the structure and morphology of the nanoparticles to give further insight into the features of the AgNPs obtained from the proposed biogenic synthesis method, the image showed relatively spherical shape of the formed nanoparticles. The EDS microanalysis is shown in Figure 5b and confirms the presence of AgNPs which is known to provide information on the chemical analysis of the elements or the composition at specific locations. The spectrum analysis reveals signal in the silver region and then confirms the formation of AgNPs. Metallic silver nanocrystals generally show a typical optical absorption peak at approximately 3 keV due to the surface plasmon resonance (Ip et al., 2006; Bar et al. 2009; Magudapathy et al., 2001). This result confirmed that the produced nano-structures are pure silver as shown in Table 1.

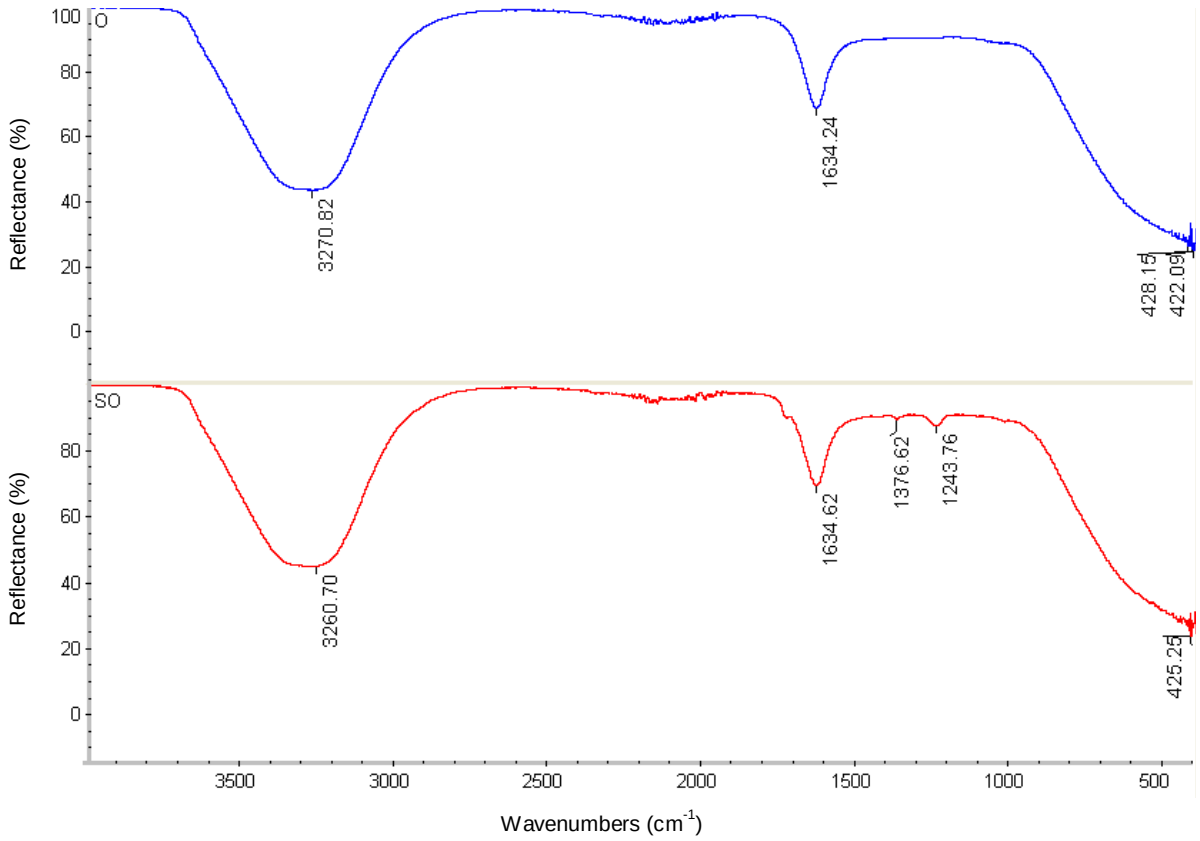

Figure 2. FTIR adsorption spectra of AgNPs prepared by orange peel.

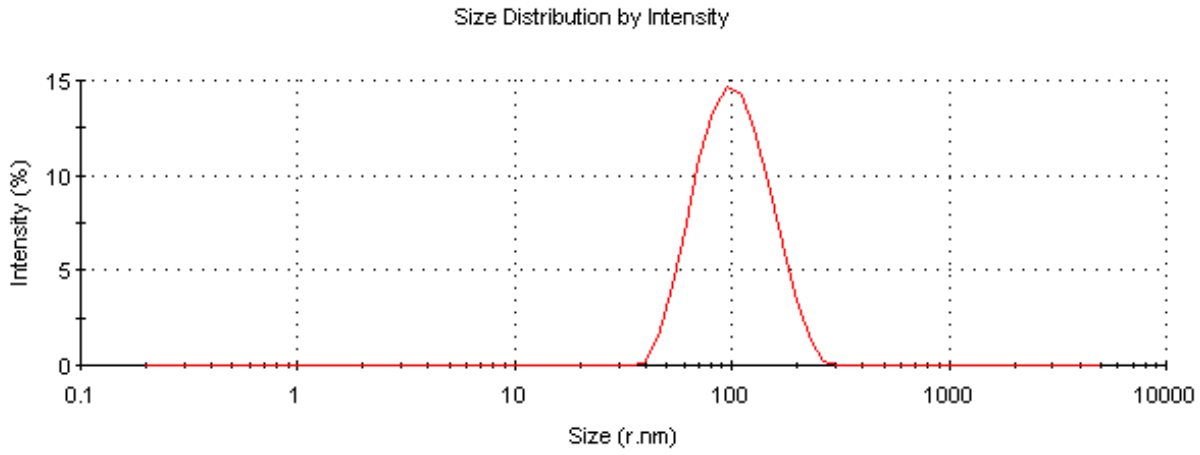

		Diam. (nm)	% Intensity	Width (nm)
Z-Average (r.nm): 91.89	Peak 1:	107.4	100.0	39.86
PdI: 0.147	Peak 2:	0.000	0.0	0.000
Intercept: 0.869	Peak 3:	0.000	0.0	0.000
Result quality : Good				

Figure 3. Zitasizer of the formed AgNPs.

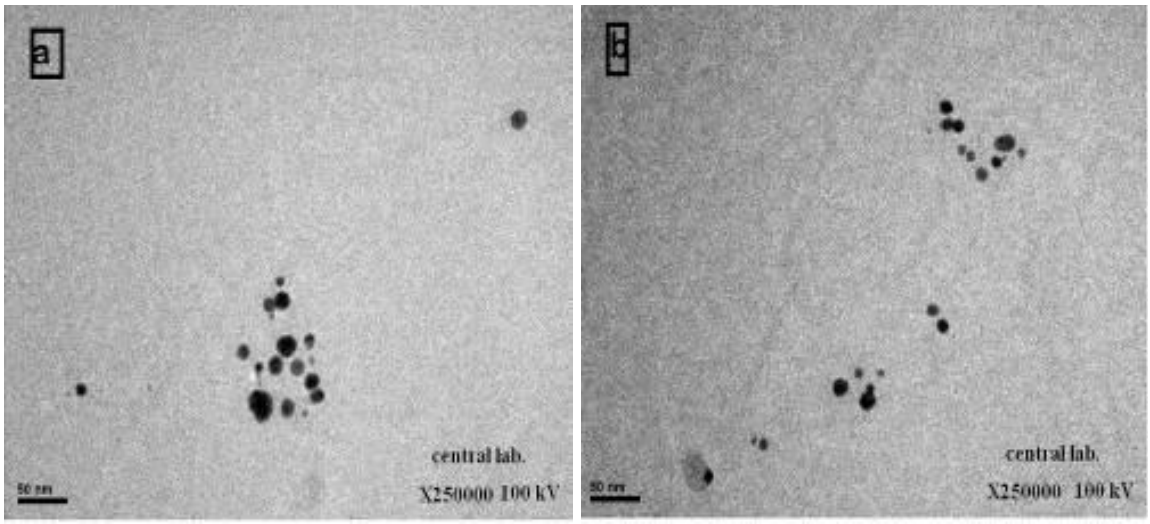

Figure 4a and b. TEM images of the formed biogenic AgNPs.

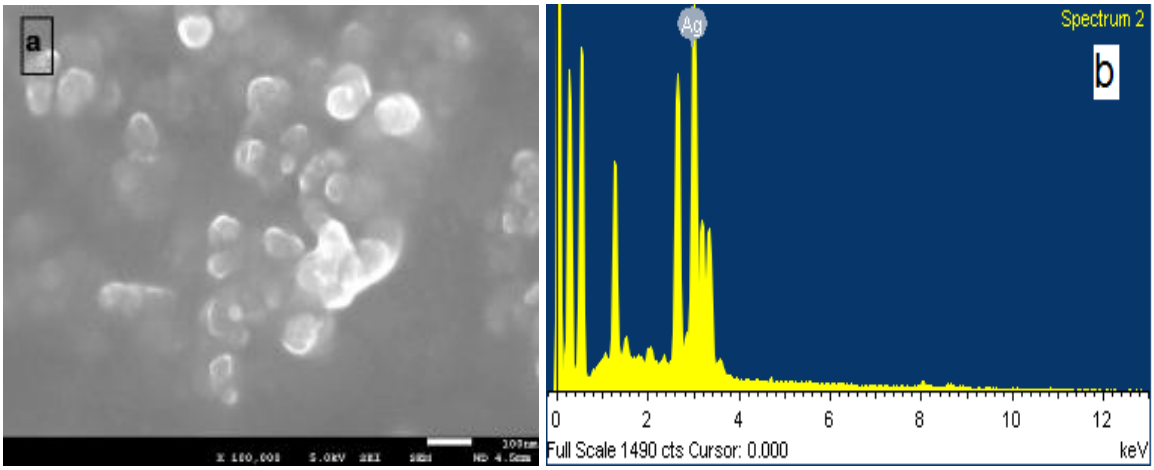

Figure 5. Green synthesis method (a) SEM image, (b) EDS pattern of spherical AgNPs prepared.

Silver nanoparticles as antibacterial agent

Silver, a naturally occurring element, is non-toxic, hypoallergenic, and does not accumulate in the body to cause harm and is considered safe for the environment. Many manufactured goods like washing machines, air conditioners and refrigerators are using linings of AgNPs for their antimicrobial qualities. Sportswear, toys and baby articles, food storage containers, HEPA filters, laundry detergent etc. are made with AgNPs. The products also with AgNPs were used, such as heart valves and other implants, medical face masks, wound dressings and bandages.

Nanomaterials are the leaders in the field of nanomedicine, bio-nanotechnology and have a great importance in nano toxicology research. Silver exhibits the strong toxicity in various chemical forms to a wide range of microorganism that is very well known and AgNPs have recently been shown to be a promising antimicrobial material (Ip et al., 2006).

In this work, the antibacterial activity of the biogenic synthesized AgNPs. The analysis results showed that nanoparticles exhibited low toxicity against *Klebsiella* which the zone of inhibition around AgNP saturated disc for bacterial culture, and the numerical value of diameter of inhibition zone was presented in Table 2, also the results showed maximum sensitivity against *E. coli*, *Pseudomonas*, and *Salmonella*.

The results in Table 2 confirmed that the successfully biogenic synthesized AgNPs showed antibacterial activity on both gram-positive and gram-negative bacteria and the analysis of bacterial growth showed that the toxicity of

Table 1. EDS elemental micro-analysis of the AgNPs.

Element	Weight (%)	Atomic (%)
Ag L	100.00	100.00
Total	100.00	

Table 2. Zone of inhibition (mm) of nanoparticles against different bacterial strains

Reagent	*E. coli* interpretation zone diameters (mm)			*Klebsiella* interpretation zone diameters (mm)			*Pseudomonas* interpretation zone diameters (mm)			*Salmonella* interpretation zone diameters (mm)		
AgNPs	6	6	6	3	2	3	6	6	6	6	6	6

AgNPs spherical shape are higher than that of gold nanoparticles spherical shape.

Hence, AgNPs synthesized by this method should be prospect further for antimicrobial applications for examples in wastewater treatment, food and water storage and manufacturing of medical supplies such as wound dressings or beds, bandages. The biological method used here in preparation is recognized by saving huge amount of energy, eco-friendly, economic, clean, and has no any toxic chemicals for the synthesis.

Conclusion

Present work demonstrated the rapid extracellular biogenic synthesis of green AgNPs using an orange peel extract and their use as an antibacterial agent. The used biogenic method here is non-toxic, environmentally friendly, simple, low cost and has no toxic chemicals. The results confirmed that orange peel plays an important role in the reduction and stabilization of silver. The formation of AgNPs was determined by UV-Vis spectroscopy where surface plasmon absorption maxima can be observed at 466 nm from the UV-Vis spectrum. Zitasizer shows the average size of the produced nanoparticles to be 91 nm. The bio produced AgNPs were characterized using FT-IR spectroscopic, TEM, SEM and EDS techniques.

For technical view, the successfully biogenic synthesized AgNPs showed antibacterial activity on both gram-positive and gram-negative bacteria and this may be useful in a wide variety of applications in pharmaceutical, biomedical fields, industrial appliances like bandage, food and water storage and wastewater treatment in a low price.

ACKNOWLEDGEMENTS

The authors extend their appreciation to the Deanship of Scientific Research at King Saud University for funding this work through research group no RGP- VPP-278.

REFERENCES

Bar H, Bhui DH, Sahoo PG, Sarkar P, De PS, Misra A (2009a). Green synthesis of silver nanoparticles using latex of Jatrapha curcas. Colloids Surf. A Physicochem. Eng. Asp. 339:134–139.

Bhyan SB, Alam MM, Ali MS (2007). Effect of plant extracts on Okra mosaic virus incidence and yield related parameters of Okra. J. Agric. Res. 1:112-118.

Calvo MA, Angulo E, Costa-Batllori P, Shiva C, Adelantado C, Vicente A (2006). Natural plant extracts and organic acids: synergism and implication on piglet's intestinal microbiota. Biotechnol. 5: 137-142.

Cao XL, Cheng C, Ma YL, Zhao CS(2010). Preparation of silver nanoparticles with antimicrobial activities and the researches of their biocompatibilities. J. Mater. Sci. Mater M 21:2861–2868.

Chandan Singh, Vineet Sharama, Pradeep KR Naik, Vikas KHandelwal, Harvinder Singh(2011). A green biogenic approach for synthesis of gold and silver nanoparticles using Zingiber officinale. Digest J. Nanomaterials Biostructures 6(2):335-542.

Dastjerdi R, Montazer M, Shahsavan S (2010). Size-controlled preparation of silver nanoparticles by a modified polyol method, Colloids Surf. A Physicochem. Eng. Aspects 366:197–202.

Du WL, Niu SS, Xu YL; Xu ZR, Fan CL (2009). Antibacterial activity of chitosan tripolyphosphate nanoparticles loaded with various metal ions. Carbohydr. Polym. 75:385–389.

Huang J, Li Q, Sun D, Lu Y, Su Y, Yang X, Wang H, Wang Y, Shao W, He N, Hong J, Chen C (2007). Biosynthesis of silver and gold nanoparticles by novel sundried Cinnamomum camphora leaf. Nanotechnology, 18:105–106.

Ip M, Lui SL, Poon VKM, Lung I, Burd A (2006). Antimicrobial activities of silver dressings: an *in vitro* comparison. J. Medical Microbial. 55:59-63.

Jeong SH, Yeo SY, Yi SC (2005). The effect of filler particle size on the antibacterial properties of compounded polymer/silver fibers. J. Mat. Sci. 40:5407-5411.

Kamyar S, Mansor BA, Seyed DJ, Parvaneh S, Parvanh S, Hossein J, Yadollah GS (2012). Investigation of antibacterial properties silver nanoparticles prepared via green method. Chemistry central J. 6:73.

Khandelwal N, Singh A, Jain D, Upadhyay M.K., Verma HN (2010). Green synthesis of silver nanoparticles using Argimone mexicana leaf extract and Evaluation of their antimicrobial activities. J. Nanomater. Biostruct. 5:483-489.

Krutyakov YA, Kudrynskiy A, Olenin AY, Lisichkin GV (2008). Extracellur biosynthesis and antimicrobial activity of silver nanoparticles. Russ. Chem. Rev.77:233-236.

Magudapathy P, Gangopadhyay P, Panigrahi BK, Nair KGM, Dhara S (2001). Electrical transport studies of Ag nanoclusters embedded in glass matrix. Physica B, 299(1-2):(142–146).

Marambio-Jones C, Hoek EMV (2010). A review of the antibacterial effects of silver nanomaterials and potential implications for human health and the environment. J. Nanopart. Res, 12:1531-1551.

Muhammad A, Farooq A, Muhammad Ramzan SAJ, Muhammad AI,

Umer R (2012). Green Synthesis of Silver Nanoparticles through Reduction with *Solanum xanthocarpum* L. Berry Extract: Characterization, Antimicrobial and Urease Inhibitory Activities against *Helicobacter pylori.* Int. J. Mol. Sci. 13:9923-994.

Palanivel V, Sang-Myung L, Mahudunan L, Kui-Jae L, Byung-Taek O (2013). Pine cone-mediated green synthesis of silver nanoparticles and their antibacterial activity against agricultural pathogens. Appl. Microbiol. Biotechnol. 97:361–368.

Savage N, Diallo MS (2005). J. Nanomaterials and water purification. opportunities and challenges. Nanopart. Res. 7:331–342.

Savithramma N, Linga RM, Rukmini K, Suvarnalatha PD (2011). Antimicrobial activity of silver nanoparticles synthesized by using medicinal plants. Int. J.Chem. Technol. Res. 3(3):1394-1402.

Saxena A, Tripathi RM, Singh RP (2010). Biological Synthesis of silver nanoparticles by using Onion (Allium cepa) extract and their antibacterial activity. J. Nanomater. Biostruct. 5:427-432.

Setua P, Chakraborty A, Seth D, Bhatta MU, Satyam PV, Sarkar N (2007). Synthesis, optical properties, and surface enhanced Raman scattering of silver nanoparticles in nonaqueous methanol reverse micelles. N. J. Phys. Chem. C. 111:3901–3907.

Sharma VK, Yngard RA, Lin Y (2009). Silver nanoparticles: Green synthesis and their antimicrobial activities. Adv. Coll. Int. Sci. 145:83-96.

Singh A, Jain D, Upadhyay MK, Khandelwal N, Verma HN, Verma HN (2010). Green synthesis of silver nanoparticles using Argemone mexicana leaf extract and evaluation of their antimicrobial activities. Dig J Nanomater Bios, 5:483–489.

Sinha S, Pan I, Chanda P, Sen SK (2009). Nanoparticles fabrication using ambient biological resources. J. Appl. Biosci. 19:1113–1130.

Thirumurgan A, Tomy NA, Jai GR, Gobikrishnan S (2010). Biological reduction of silver nanoparticles using plant leaf extracts and its effect an increased antimicrobial activity against clinically isolated organism. Phar. Chem. 2:279-284.

Thirumurguan G, Shaheedha SM, Dhanaraju MD (2009). *In vitro* evaluation of antibacterial activity of silver nanoparticles synthesized by using phytothora infestans. Int. J. Chem Tech Res. 1:714-716.

Yugang S, Mayers B, Xia YP (2003). Synthesis of uniform silver nanowires: A plausible growth mechanism and the supporting evidence. Nano Lett. 3:955–960.

academicJournals

Vol. 9(3), pp. 41-47, 9 February, 2014
DOI: 10.5897/IJPS2013.4101
ISSN 1992 - 1950 © 2014 Academic Journals
http://www.academicjournals.org/IJPS

International Journal of Physical Sciences

Full Length Research Paper

Development of a multilayer perceptron (MLP) based neural network controller for grid connected photovoltaic system

A. Ndiaye*, L. Thiaw, G. Sow and S. S. Fall

Laboratory of Renewable energy, Polytechnic Higher School, Cheikh Anta Diop University BP 5085, Dakar, Senegal.

Accepted 29 January, 2014

This paper focuses on the development of a controller for grid connected photovoltaic energy conversion system. Control design of a single phase inverter interfacing a photovoltaic generator and an electrical grid is performed, based on Artificial Neural Networks. The developed controller is compared with a Proportional Integral (PI) controller through computer simulation. The obtained results show that the neural controller has faster response and lower total harmonic distortion (THD) without overshoots.

Key words: Photovoltaic generator, inverter, maximum power point tracking (MPPT), neural networks.

INTRODUCTION

The main difficulties in the control strategy of real dynamic systems are the non-linearity and strong non-linearity. The lack of right knowledge necessary for the development of the uncertainties. The control of the system requires in general the development of a mathematical model making it possible to establish the transfer function of the system that links the inputs and the outputs. This requires good knowledge of the dynamic and properties of the system. In the non-linear system case, the conventional techniques have often shown their limits mainly when the system to be studied presents mathematical models is somehow the origin of those limits (Mohammed et al., 2007).

Recourse to the control methods based on artificial intelligence has become a necessity. These control methods follow an extraction process of the knowledge of the system to be studied from collected empirical data, so as to be able to react in front of new situations: This strategy is known as intelligent control (Panos et al., 1993).

Artificial neural networks are used in intelligent control due to the fact that they are parsimonious universal approximators (Panos et al., 1993; Rival et al., 1995) and that they have the capacity to adapt to a dynamic evolving through time. Moreover, as multi-input and multi-output systems, they can be used in the frame of the control of the multivariable systems.

A feed forward ANN makes one or more algebraic functions of its inputs, by the composition of the functions made by each one of its neurons (Dreyfus, 2002). These are organized in layers and inter-connected by well-balanced synaptic connections. The supervised training of a neural network consists in modifying the weights to have a given behavior minimizing a cost function often represented by the quadratic error (Panos et al., 1993; Cybenko, 1989).

Several authors have tried to exploit the advantages of neural networks to control a dynamic system (Mahmoud et al., 2012; Zameer and Singh, 2013) precisely, within the field of robotics (Rival et al., 1995; Yildirim, 1997) and

*Corresponding author. E-mail: alphousseynou.ndiaye@ucad.edu.sn.

for the control of asynchronous motors (Mohammed et al., 2007; Panos et al., 1993; Branštetter and Skotnica, 2000). More details on neural network controllers can be found in Panos et al. (1993), Wishart and Harley (1995), Ronco and Gawthrop (1997), Hagan and Demuth (1996), Wishart and Harley (1995), Ahmed et al. (2008), Tai et al., (1990), Hagan and Demuth (1996), Chen et al. (1997), Norgaard (1996) and Vandoorn et al. (2009) in which a comparative study was made between PI controller, PID controller and a fuzzy logic based controller for an inverter control shows that the PI controller has better performances, though the fuzzy logic based controller is an intelligent one.

In the work presented in this article, the capacities of multi-layer perceptron (MLP) to learn the inverse model of non-linear systems are used to work out the control of a single-phase inverter used as an interface between a photovoltaic generator (PVG) and an electrical grid. The objective is to inject into the grid as much photovoltaic energy as available, with low total harmonic distortion (THD) and good reference signal tracking a characteristic.

METHODOLOGY

Inverter control by using a PI controller

The PI controller is the most used controller in industrial systems. It is easy to implement and it is costs efficient. The control scheme of a grid connected photovoltaic system used in this work is given in Figure 1.

A loop control is elaborated in order to ensure the injection of the maximum available photovoltaic energy into the grid. This loop enables current control to give a reference current determined by the maximum power point tracking system (Figures 1 and 2). In order to determine the controller parameters, the whole system model has been established. The inverter transfer function links inverter output current to the duty cycle. The PI controller parameters can be determined from this transfer function. The input voltage of the inverter is supposed to be constant (ripple are neglected). From Figure 1, Equation (1) can be established.

$$\mathrm{L_{ac}}\frac{di_g}{dt} = \alpha V_{dc} - v_g \quad (1)$$

Where, L = inductor value of the filter; i_g = current injected into the grid; α = duty cycle; V_{dc} = inverter input voltage, and v_g = grid voltage;
Using small signals models, it is possible to write:

$$\alpha = \overline{\alpha} + \widetilde{\alpha}$$
$$I_g = \overline{I} + \widetilde{i_g}$$

Where, $\overline{\alpha}$ is the average value of the duty cycle and $\widetilde{\alpha}$ the duty cycle ripple; $\overline{I}_g$ is the average value of the current and $\widetilde{i_g}$ the current ripple.
Considering that the grid average voltage is null and neglecting its ripples, Equation (2) can be obtained.

$$\frac{d\widetilde{i_g}}{dt} = \frac{V_{dc}}{L}\widetilde{\alpha} \quad (2)$$

Applying Laplace transform to Equation (2) and considering the control loop represented in Figure 2, we get the open loop transfer function expressed by Equation (3) linking the injected current to the duty cycle.

$$\mathrm{G_g} = \left(k_p + \frac{k_i}{s}\right)\frac{G_{ti}}{v_{ti}}\frac{V_{dc}}{sL} \quad (3)$$

Where, v_{ti} = The magnitude of the carrier, and G_{ti} = gain loop (gain of the current sensor).
Exploiting this transfer function allows the PI coefficients to be determined (Equations 4 and 5).

$$\mathrm{k_p} = \frac{2\pi f_{cL} L v_{ti}}{V_{dc} G_{ti}} \quad (4)$$

$$\mathrm{k_i} = \frac{2\pi f_{cL}}{\tan(p_{hm})} \quad (5)$$

Where, f_{cL} = Cut-off frequency, and p_{hm} = Phase margin.
The PI controller input consists of the error between the current provided by the inverter and its reference. The objective of this control is to correct the current injected into the grid (i_g) so that it follows the reference value (i_{gref}).
This type of controllers is simple but it gives limited performances if the system integrates strongly nonlinear elements such as static inverters. In fact, the determination of the controller parameters can be done through different methods but generally depends on the knowledge of the system to be controlled, and mathematical model of the system is not always available. Equations 4 and 5 show that the parameters of the PI controller (kp and ki) depend on Vcd which is related to meteorological conditions (solar irradiation and temperature). So it is worth adapting this coefficient any time the meteorological conditions change, which seems to be impossible. Therefore an adaptive control has to be set up. This fact has led to carrying out a comparative study of a PI controller and a neural network controller.

Neural network controller for single phase inverter

Principles of artificial neural networks

The ANN network is based on models that try to explain human brain functioning. They are adapted to the treatment in parallel of complex problems such as speech and face recognition, or simulation of nonlinear functions. So they offer a new means of information treatment. In Figure 3, the main elements of an artificial neural are depicted: the input, processing unit and an output.
A formal neuron is characterized by Equations (6) and (7).

$$x_i = f(A_i) \quad (6)$$

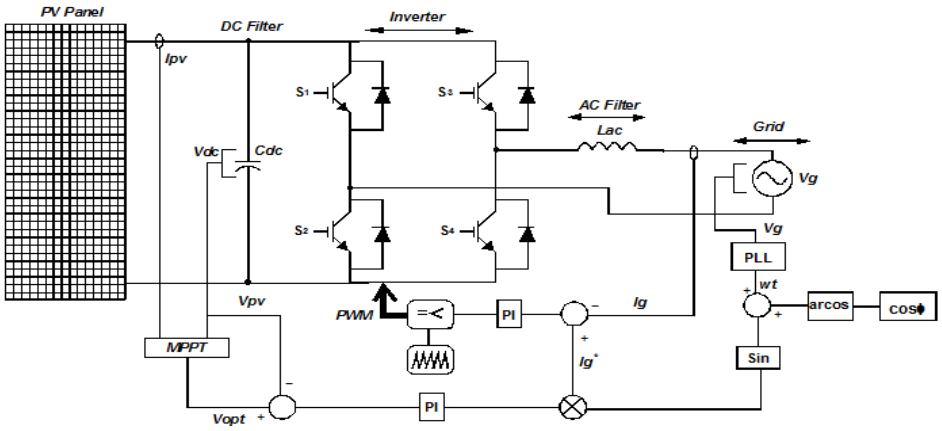

Figure 1. Control loop of a grid connected photovoltaic system.

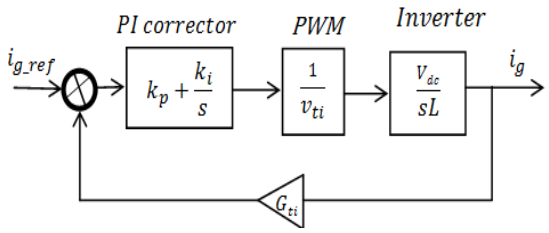

Figure 2. Control loop of the inverter current.

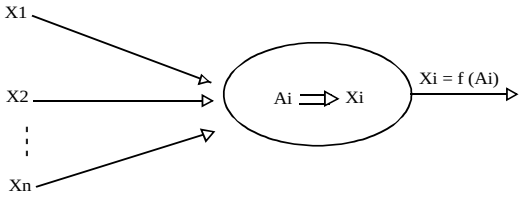

Figure 3. Representation of a formal neuron.

$$A_i = \sum_{i=1}^{N_i} w_{ij} x_i + b_i \quad (7)$$

With, x_i = State of a neuron j connected to neuron i; A_i = Activity of neuron i; w_{ij} = Weight of the connexion between the neurons j and I, and b_i = Bias.

The MLP network (Figure 4) is a feed forward network that is composed of several layers, each neuron of a layer being totally connected to the neurons of the next layer. The resulting network is able to approximate any nonlinear function.

The error $\delta_{p,k}$ made on the k[th] output neuron for a sample p is expressed by Equation (8).

$$\delta_{p,k} = O_{p,k} - x_{p,k} \quad (8)$$

Where, $O_{p,k}$ = Desired output of the neuron k for the sample p, and $x_{p,k}$ = output of the neuron k for the sample p.

As a result, the total error (for all output neurons) is estimated by:

$$e_p = \frac{1}{2}\sum_{i=1}^{N_i} \delta_{p,k}^2 = \frac{1}{2}\sum_{k=1}^{m} \left(O_{p,k} - x_{p,k}\right)^2$$

Where m = number of neurons on the output node.

The synaptic weights are then adjusted so as to reduce the output error for the whole samples of the data base:

$$e = \sum_{p=1}^{N} e_p \quad (9)$$

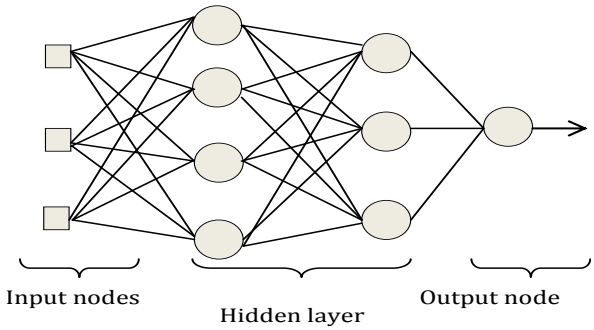

Figure 4. Architecture of an MLP network.

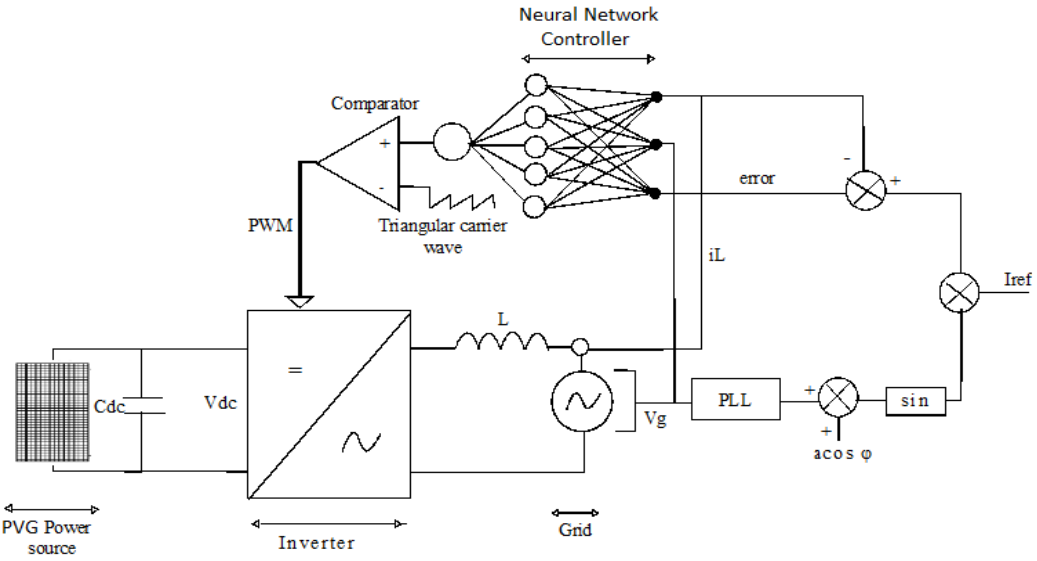

Figure 5. Grid connected photovoltaic system with single phase inverter and neural controller.

Where N designates the size of the database.

The process of the network parameters estimation is called training. The set of parameters that are to be estimated includes all the weights and biases. An algorithm called back propagation is mainly used for the network training. More details on neural networks is given in Ahmed et al. (2008).

Proposed design method of the neural controller

Within the framework of this study, the system to control is a single-phase inverter serving as an interface between a photovoltaic generator and an electrical grid. The structure of the neural controller for photovoltaic energy injection into the grid is represented in Figure 5.

The inputs of the neural controller are the current injected into the grid, the grid voltage and the error between the actual and the reference values of the inverter output current.

Database for the neural controller training is obtainend from the system simulation with several PI controllers, each of witch being determined for a given system operating point, defined by the inverter input DC voltage.

RESULTS AND DISCUSSION

The inverter is designed so that its switches be able to support the maximum current i_{gmax} and the maximum open circuit voltage (Vco) of the photovoltaic generator. Table 1 gives the inverter parameters and those of the photovoltaic generator.

The filter inductor value is determined by Equation (11).

$$L = \frac{V_{dc}}{16 \Delta I_{max} f_s} \quad (11)$$

Where, *Vcd*. is the inverter input voltage; f_s is the switching frequency, and ΔI_{max} is the maximum value of the output current ripple.

The system is first simulated with the PI controller (Table 2). The injected current and its reference value are presented in Figure 6, whereas Figure 7 shows grid

Table 1. Inverter and photovoltaic generator parameters.

Parameter	Value
DC bus voltage (Vdc = Vopt at 1 kW/m² and 25°C)	800 V
Opened circuit voltage of the PV generator	1000 V
Short circuit current of the PV generator	6.8 A
Filter inductor value (L)	5 mH
ESR value of the inductor	0.2 Ω
Maximum power of the PV generator	4 kW
Grid RMS voltage value (Vgeff)	220 V
Grid frequency (f_o)	50 Hz
Inverter switching frequency (fs)	20 kHz

Table 2. PI controller parameters.

Coefficients	kp	ki
Values	5.23	6.33 104

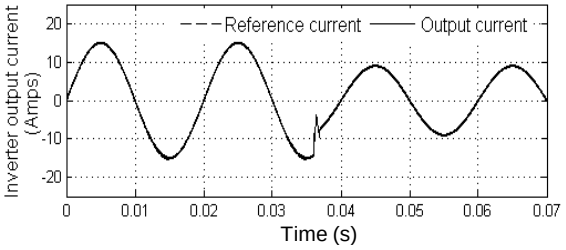

Figure 6. Inverter output current and its reference value when a PI controller is used.

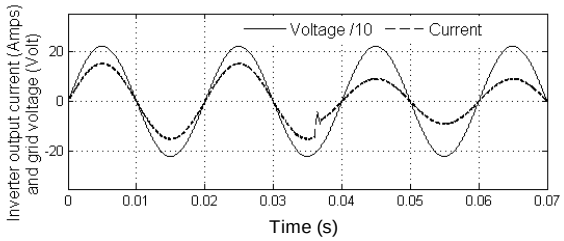

Figure 7. Grid voltage and inverter output current when a PI controller is used.

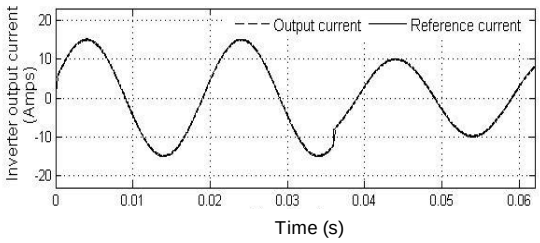

Figure 8. Inverter output current and its reference value when a neural controller is used.

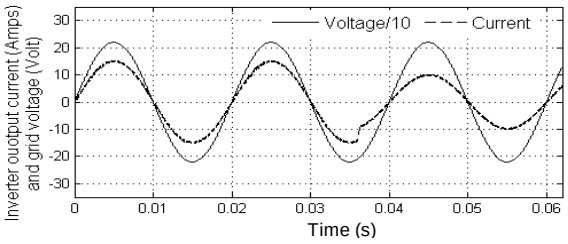

Figure 9. Grid voltage and inverter output current when a neural controller is used.

voltage and injected current for unity power factor. A disturbance consisting of a 33% reduction of reference current magnitude is introduced at t = 36 ms. The PI controller presents a relatively fast reference current tracking but an important overshoot can be noticed. The main drawbacks of this controller is due to the fact that it has to be designed for a given meteorological conditions.

The design of the neural network controller consists of designing several PI controllers for various meteorological conditions. The following values are used for the solar irradiation and the temperature: (0.25 kW/m², 25°C), (0.25 kW/m², 40°C), (0.6 kW/m², 25°C), (0.6 kW/m², 40°C), (1 kW/m², 25°C) and (1 kW/m², 40°C).

Control signals from the PI controllers, grid voltage, inverter output current and its reference value are gathered to form a large database used for the neural controller training.

Figure 8 shows inverter output current and its reference value when neural controller is used for the following meteorological conditions: a solar irradiation of 1 kW/m² and a temperature of 25°C. A disturbance consisting of a 33% reduction of reference current magnitude is introduced at t = 36 ms. The obtained results prove fast tracking capability of the neural controller without overshoots. Grid voltage and injected current for unity power factor are shown in Figure 9.

A comparison study of the two controllers is performed throughout simulation of two cases. In the first case, the simulation is made for the following meteorological conditions: Solar irradiation of 1 kW/m^2 and temperature of 50°C. The PI controller parameters for these meteorological conditions has resulted in kp=1.16 and ki=7.07 10^3 rad/s.

The total harmonic distortion (THD) of both controllers have been calculated and compared. The obtained results are presented on Figures 10 and 11. They show that the neuronal controller has a THD slightly weaker than the PI controller.

In the second simulation case, the same meteorological conditions were used but a disturbance consisting in a rapid variation of the reference current has been introduced. The simulation results are represented on Figures 12 and in Table 3. These results show that the relative error between the injected current and its

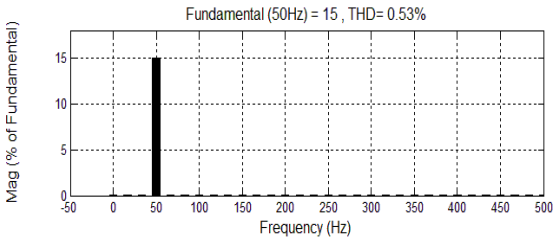

Figure 10. THD obtained with a PI controller for a solar irradiation of 1 kW/m^2 and a temperature of 50°C.

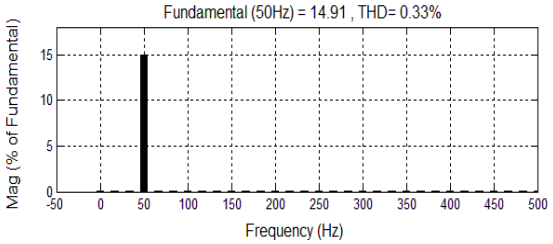

Figure 11. THD obtained with the neural controller for a solar irradiation of 1 kW/m^2 and a temperature of 50°C.

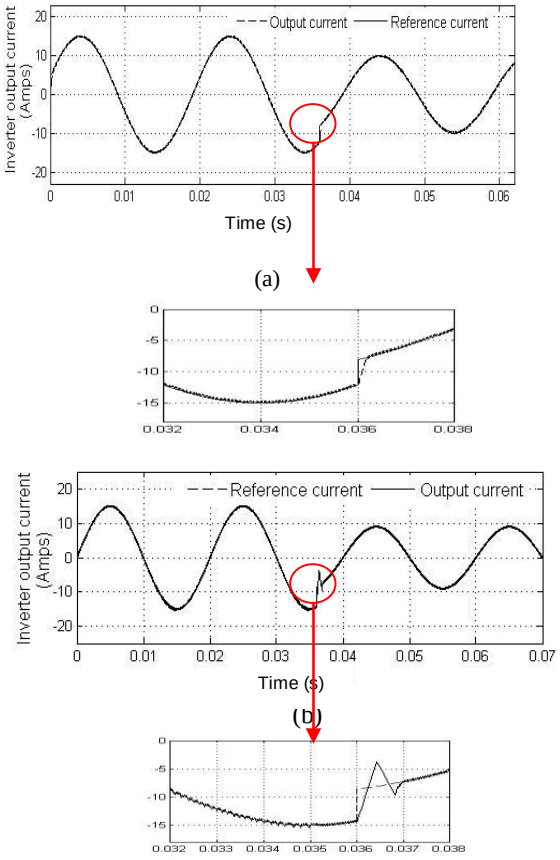

Figure 12. Performances of the neuronal controller (a) and PI controller of (b) with disturbance, for an irradiation of 1 kW/m^2 and a temperature of 50°C.

Table 3. Comparison results of the pi and neural controller.

Performance	Neural controller	PI controller
Time response (ms)	0.5	1
Overshoot current (A)	0	5
Total harmonic distortion (%)	0.33	0.53
Magnitude of the fundamental current (A)	14.96	15
Relative current error: 100*(ig-ig_ref) /Ig_refmax	0.67	1.33

reference is weaker for the neural controller, be it the half of the one obtained by PI controller. Moreover, the PI controller has a response time twice greater than that of the neural controller. Unlike the PI controller, the neural controller responds to the disturbance without overshoot. These two controllers provide a fundamental magnitude of about 15 A. Yet, considering the nature of both signals, the neural controller gets closer to the reference, giving its weak THD (Figures 10 and 11).

Conclusion

Development of a MLP based neural controller is presented. The training and validation data of the used neural controller were obtained by simulation of the whole system with several PI controllers calculated for various meteorological conditions. The simulation results show that the neural controller gives better results than a PI controller. The advantage of neural network based controller is that it adapts to the changing of meteorological conditions unlike the PI controller whose performance decreases during a strong variation of the temperature and/or irradiation.

REFERENCES

Ahmed T, Hamza A, Abdel GA (2008). La commande neuronale de la machine à réluctance variable'' Rev. Roum. Sci. Techn. – Électrotechn. et Énerg. Bucarest. 53(4):473–482.

Branštetter P, Skotnica M (2000). Application of artificial neural network for speed control of asynchronous motor with vector control, Proceedings of International Conference of Košice, EPE-PEMC, 6-157-6-159.

Chen CT, Chang WD, Hwu J (1997). Direct control of nonlinear dynamical systems using an adaptive single neuron, IEEE Trans on Neural Networks 2(10):33-40.

Cybenko G (1989). Approximation by superposition of a sigmoidal function'', Math. In: Control Signals System 2nd ed, pp. 303-314.

Dreyfus G (2002). Réseaux de neurones: méthodologies et applications, editions Eyrolles.

Hagan MT, Demuth HB (1996). Neural network design, Thomson Asia Pte Ltd, 2nd ed.

Mohammed S, Djamel E, Chaouch M, Fayçal K (2007). Commande neuronale inverse des systèmes non linéaires, In 4th International Conference on Computer Integrated Manufacturing CIP, 2007 03-04 November.

Mahmoud AY, Tamer K, Mushtaq N, Mohd AA (2012). An Improved Maximum Power Point Tracking Controller for PV Systems Using Artificial Neural Network, Przegląd Elektrotechniczny (Electrical Review), ISSN 0033-2097, R. 88 NR 3b/2012.

Norgaard M (1996). System identification and control with neural networks'', Thesis, Institute of automation, Technical University of Denmark.

Panos J, Antsaklis K, Passino M (1993). Introduction to Intelligent and Autonomous Control, Kluwer Academic Publishers, ISBN: 0-7923-9267-1.

Rival I, Personnaz L, Dreyfus G (1995). Modélisation, classification et commande, Par réseaux de neurones: principes fondamentaux, Méthodologie de conception et illustrations industrielles, Mécanique Industrielle et Matériaux, n°51 (septembre 1998).

Ronco E, Gawthrop PJ (1997). Neural networks for modelling and control, Techncal Report CSC-97008, Center for Systems and Control, Glasgow.

Tai P, Ryaciotaki-Boussalis HA, Tai K (1990). The application of neural networks to control systems: a survey, Signals, systems and Computers, Record Twenty-Fourth Asilomar Conference on Vol.1.

Vandoorn T, Renders B, De Belie F, Meersman B, Vandevelde L (2009). A Voltage-Source Inverter for Microgrid Applications with an Inner Current Control Loop and an Outer Voltage Control Loop, International Conference on Renewable Energies, and Power Quality (ICREPQ09) Valencia (Spain), 15th to 17th April.

Wishart MT, Harley RG (1995). Identification and Control of Induction Machines Using Artificial Neural Networks, IEEE Transaction on Industry Applications, 31:3.

Yildirim S (1997) New neural networks for adaptive control of robot manipulators, Neural Networks, International Conference. 3:1727–1731.

Zameer A, Singh SN (2013). Modeling and Control of Grid Connected Photovoltaic System-A Review, Int.J. Emerging Technol. Adv. Eng. ISSN 2250-2459, ISO 9001:2008. 3(3).

academicJournals

Related Journals Published by Academic Journals

■African Journal of Pure and Applied Chemistry

■Journal of Internet and Information Systems

■Journal of Geology and Mining Research

■Journal of Oceanography and Marine Science

■Journal of Environmental Chemistry and Ecotoxicology

■Journal of Petroleum Technology and Alternative Fuels